ErbB2-NOTCH1 axis controls autophagy in cardiac cells

Francesca Fortini[1*], Francesco Vieceli Dalla Sega[1*], Edoardo Lazzarini[2,3*], Giorgio Aquila[4], Polina Sysa-Shah[5], Edoardo Bertero[6], Alessia Ascierto[4], Paolo Severi[4], Achille Wilfred Ouambo Talla[4], Alessio Schirone[7], Kathleen Gabrielson[8], Giampaolo Morciano[1,9], Simone Patergnani[9], Gaia Pedriali[1], Paolo Pinton[1,9], Roberto Ferrari[4], Elena Tremoli[1], Pietro Ameri[6,10§] and Paola Rizzo[1,4§]

[1] Maria Cecilia Hospital, GVM Care & Research, Cotignola, Ravenna, Italy;
[2] Laboratory for Cardiovascular Theranostics, Cardiocentro Ticino Institute, Ente Ospedaliero Cantonale Lugano, Switzerland;
[3] Euler Institute, Faculty of Biomedical Sciences, Università della Svizzera italiana, Lugano Switzerland;
[4] Department of Translational Medicine and Laboratory for Technologies of Advanced Therapies (LTTA), University of Ferrara, Ferrara, Italy;
[5] The Brady Urological Institute and Department of Urology, Johns Hopkins University, School of Medicine, Baltimore, Maryland, USA;
[6] Department of Internal Medicine and Specialties (Di.M.I.), University of Genova, Italy;
[7] Oncology and Hematology Department, Azienda Ospedaliero-Universitaria di Ferrara, Italy;
[8] Department of Molecular and Comparative Pathobiology, Johns Hopkins University School of Medicine; Department of Pathology, Johns Hopkins University School of Medicine; Sidney Kimmel Comprehensive Cancer Center, Johns Hopkins University, Baltimore, Maryland, USA;
[9] Department of Medical Sciences, University of Ferrara, Ferrara, Italy;
[10] Cardiac, Thoracic, and Vascular Department, IRCCS Ospedale Policlinico San Martino, Genova, Italy.

* These authors have contributed equally to this work and share first authorship

[§] These authors share senior authorship

Correspondence:

Francesca Fortini (ffortini@gvmnet.it)

Paola Rizzo (rzzpla@unife.it)

Abstract

Although the epidermal growth factor receptor 2 (ErbB2) and Notch1 signaling pathways have both significant roles in regulating cardiac biology, their interplay in the heart remains poorly investigated. Here, we present evidence of a crosstalk between ErbB2 and Notch1 in cardiac cells, with effects on autophagy and proliferation. Overexpression of ErbB2 in H9c2 cardiomyoblasts induced Notch1 activation in a post-transcriptional, p38-dependent manner, while ErbB2 inhibition with the specific inhibitor, lapatinib, reduced Notch1 activation. Moreover, incubation of H9c2 cells with lapatinib resulted in stalled autophagic flux and decreased proliferation, consistent with the established cardiotoxicity of this and other ErbB2-targeting drugs. Confirming the findings in H9c2 cells, exposure of primary neonatal mouse cardiomyocytes to exogenous neuregulin-1, which engages ErbB2, stimulated proliferation, and this effect was abrogated by concomitant inhibition of the enzyme responsible for Notch1 activation. Furthermore, the hearts of transgenic mice specifically overexpressing ErbB2 in cardiomyocytes had increased levels of active Notch1 and of Notch-related genes. These data expand the knowledge of ErbB2 and Notch1 functions in the heart and may allow better understanding the mechanisms of the cardiotoxicity of ErbB2-targeting cancer treatments.

Running title

ErbB2-NOTCH1 interaction in cardiac cells

Keywords

ErbB2; Notch; autophagy; cardiomyocytes; heart

1 INTRODUCTION

ErbB2 (HER2, human epidermal growth factor receptor 2, in human) is a member of the epidermal growth factor receptor (EGFR) family with major roles in cardiac development, preservation of homeostasis, and response to stress (1). In the postnatal heart, the action of ErbB2 is mostly related to the formation of heterodimers with another EGFR, ErbB4, following binding of the latter by neuregulin-1 (NRG-1), with ensuing initiation of protective signaling pathways (2).

Numerous studies have shown that ErbB2 inhibition impairs the function and survival of cardiomyocytes by affecting mitochondrial function (3, 4) and metabolism (5), promoting apoptosis (6, 7). ErbB2 inhibition in cardiomyocytes causes increased oxidative stress (8, 4), while its overexpression upregulates antioxidant enzymes and reduces basal levels of reactive oxygen species (ROS), protecting against doxorubicin-induced cardiotoxicity (9). It has also been suggested that disruption of ErbB2-driven signaling leads to dysregulated autophagy, which is particularly crucial for maintaining tissue homeostasis in post-mitotic cells, such as cardiomyocytes, by recycling cellular components and damaged organelles (10, 11). Based on this evidence, defective ErbB2 activity has been implicated in cardiac disease.

The importance of ErbB2 in cardiac biology - and of ErbB2 blockade in cardiac pathology - was discovered after finding an unexpectedly high rate of left ventricular dysfunction and heart failure (HF) in pivotal clinical trials testing trastuzumab, a monoclonal antibody against HER2, in patients with breast cancer. Approximately 20% of human breast cancers overexpress HER2, which is constitutively activated and promotes cell cycle progression and proliferation in a ligand-independent manner (12). Hence, HER2-expressing breast cancer is more aggressive and confers a poorer prognosis than HER2-negative breast cancer (13). Consequently, trastuzumab and more recent HER2-targeting drugs, including pertuzumab, another monoclonal antibody, and lapatinib, a tyrosine kinase inhibitor (TKI), improve outcomes in patients with HER2-positive breast cancer. However, off-target blockade of HER2 in the heart may cause cardiotoxicity (14).

It is notable that the negative effects of therapies against HER2 cannot be solely explained by interference with the NRG-1/HER2-HER4 axis. According to their pharmacokinetics, trastuzumab, pertuzumab and lapatinib are predicted to variably affect the heterodimerization of HER2 with HER4 and may even act irrespective of ligand occupancy of the receptor (15). Furthermore, trastuzumab elicits modifications in human pluripotent stem cell-derived cardiomyocytes in the absence of exogenous NRG-1 (16).

In breast cancer cells, ErbB2 inhibition modulates Notch1 signaling (17, 18). Notch1 is one of four receptors (Notch1, 2, 3, and 4) located on the plasma membrane and activated in a juxtacrine manner by five ligands present on the surface of adjacent cells, namely Delta-like (Dll)-1, -3, and -4, and

Jagged-1 and -2. In the so-called canonical pathway, the binding of a ligand triggers two proteolytic cleavages of the Notch receptor, the second being mediated by γ-secretase. This results in the release of the active form of Notch (Notch intracellular domain, NICD), which translocates into the nucleus and regulates the transcription of several genes, including the *HES* (Hairy and Enhancer of Split) and *HEY* (Hairy and Enhancer of Split with YRPW) genes family. In the non-canonical pathway, Notch is activated even in the absence of established ligands or NICD activates/inhibits cytoplasmic proteins (19).

The Notch pathway is crucial for heart development. It is turned off in adult cardiomyocytes, but can be re-activated following injury to induce survival, proliferative, and regenerative signaling (20) by regulating mitochondrial function (21), reducing oxidative stress (22), controlling the proliferation and differentiation of cardiomyocytes (23, 24), preventing cardiomyocyte apoptosis (25-27), and reducing fibrosis (28).

Unlike in breast cancer, the crosstalk between ErbB2 and Notch1 has not been investigated in cardiac cells. We sought to bridge this gap in knowledge by investigating whether Notch1 is modulated by ErbB2 in H9c2 cardiomyoblasts and cardiomyocytes and elucidating the potential cellular functions regulated by the ErbB2/Notch1 axis.

2 EXPERIMENTAL PROCEDURES

2.1 Materials

Antibodies used were: goat polyclonal to Notch1 (C-20, catalog number sc-6014), which recognizes the C-terminus of the protein, identifying all forms of Notch1, from Santa Cruz Biotechnology (Santa Cruz, CA, USA); rabbit polyclonal to caspase-3 (catalog number #9662), rabbit monoclonal to cleaved Notch1 valine 1744 (an antibody directed against valine-1744 at the N-terminus of the cleaved form of Notch1, catalog number #4147), rabbit monoclonal to phospho-p38 MAPK (Thr180/Tyr182) (D3F9) (catalog number #9211), rabbit polyclonal to p38 MAPK (catalog number #9212) rabbit polyclonal to phospho-Akt (Ser473 catalog number #9271), rabbit polyclonal to Akt (catalog number #9272), rabbit monoclonal to phospho-p44/42 MAPK (Erk1/2) (Thr202/Tyr204) (D13.14.4E) (catalog number #4370), rabbit monoclonal to p44/42 MAPK (Erk1/2) (137F5) (catalog number #4695), rabbit monoclonal to phospho-SAPK/JNK (Thr183/Tyr185) (98F2) (catalog number #4668), rabbit monoclonal to SAPK/JNK (catalog number #9252) from Cell Signaling Technology (Beverly, MA, USA); rabbit monoclonal antibody to Bax (catalog number ab32503), rabbit polyclonal antibody to Bcl-2 (catalog number ab196495) and rabbit monoclonal antibody to Ki67 (catalog number ab16667) from Abcam (Cambridge, UK); mouse monoclonal antibody to β-actin (AC-15, catalog number A5441), rabbit polyclonal antibody to p62/SQSTM1 (catalog number

P0067) and rabbit polyclonal antibody to LC3 B (catalog number L8918) from Sigma Aldrich (St. Louis, MO, USA). Dulbecco's Modified Eagle Medium (DMEM) was from Euroclone (Milan, Italy). Fetal Bovine Serum (FBS), DAPI ProLong, Lipofectamine LTX, Opti-MEM reduced- serum medium, Annexin V-FITC, propidium iodide (PI), mitoSOX, SuperScript III reverse transcriptase, random hexamers, dNTPs, primers for RT-PCR, RNaseOut and, RNAse A were from ThermoFisher Scientific (Waltham, MA, USA). Trans-Blot® Turbo™ Mini Nitrocellulose Transfer Packs, Clarity™ Western ECL Substrate, Precast Protein Gels, 10x Tris/Glycine/SDS were from BioRad (Hercules, CA, USA). RNeasy Mini Kit was from Qiagen (Hilden, Germany). PerfeCta SYBR Green SuperMix with ROX kit was from Quanta Biosciences (Gaithersburg, MD). β-Galactosidase staining kit was purchased from Cell Signaling Technology (Beverly, MA; USA). MK-0752 and SP600125 were purchased from MedChemExpress (Monmouth Junction, NJ, USA). Lapatinib, γ- secretase inhibitor DAPT, SB203580, tetramethylrhodamine methyl ester (TMRM), carbonyl cyanide p-trifluoromethoxyphenylhydrazone (FCCP), and other materials were purchased from Sigma Aldrich (St. Louis, MO, USA).

2.2 Methods

2.2.1 Cell culture: H9c2 rat cardiomyoblasts were purchased from America Tissue Type Collection (ATCC, Manassas, VA). Cells were cultured in Dulbecco's Modified Eagle Medium (DMEM) supplemented with 10% FBS and incubated at 37°C in 5% CO_2 atmosphere. 1% penicillin / streptomycin was added in the medium. H9c2 were seeded at a density of $1x10^4/cm^2$ and used for experiments when they were 70–80% confluent.

2.2.2 Transfection with plasmids: H9c2 cells were transfected with 0.5 µg/mL of pcDNA3 vector encoding Notch1ICD (N1ICD, a gift from Dr. Lucio Miele, LSU Health Sciences Center School of Medicine, New Orleans, Louisiana), 1 µg/mL of pcDNA3 vector encoding ErbB2 or the empty vector as control (pcDNA3 CTRL), using Lipofectamine LTX (ThermoFisher Scientific). Cell treatment with lapatinib 5 µM or SB203580 10 µM began 18h after transfection. The concentration of lapatinib used for treatments was determined based on published studies in H9c2 cells (29) and clinical studies (30).

2.2.3 Proliferation assay: H9c2 cells were stained with Trypan blue 24h, 48h, and 72h after adding lapatinib 5 µM and were counted in a Burker chamber.

2.2.4 Apoptosis: Apoptosis was assessed with the Annexin V-FITC binding assay as previously described (31). Briefly, H9c2 cells were grown in the presence of treatment, then collected and stained

with Annexin V-FITC (ThermoFisher Scientific) (100 ng/ml) and PI (ThermoFisher Scientific) (10 μg/ml). Flow cytometric analysis and data analysis were performed with Attune Nxt Flow cytometer and Attune Nxt Software (ThermoFisher Scientific), respectively. Apoptosis levels were expressed as percentages of Annexin-V positive cells out of the total number of cells. As a technical positive control, we treated H9c2 with 1 μM staurosporine for 6h.

2.2.5 β-Galactosidase staining: Senescence-associated β-galactosidase (SA-β-gal) activity was determined using a Senescence β-Galactosidase staining kit (Cell Signaling), following the manufacturer's protocols. Briefly, H9c2 cells were fixed for 15 min at room temperature and then treated with β-Galactosidase Staining Solution and incubated at 37°C overnight in a dry incubator without CO_2. Senescence was quantitated by visually inspecting blue stained cells under a microscope (Nikon Eclipse Ts2) using 10X objectives. Results were expressed as the mean of blue-stained cells counted in 5 visual fields of three independent experiments. As a technical positive control, we treated human umbilical vein endothelial cells (HUVECs), cultured as previously described (32), with 0.1 μM of doxorubicin for 72h.

2.2.6 Immunofluorescence: For immunofluorescence analysis, H9c2 cells were fixed in 4% PFA. Cells were permeabilized, blocked, and then incubated overnight at 4°C with rabbit anti-Ki67. Following 3 washes, the cells were incubated for 1 hour at room temperature in the dark with anti-rabbit antibody conjugated with Alexa Fluor 633 (ThermoFisher Scientific) and then mounted with DAPI ProLong. The images were acquired using a confocal microscope (Nikon A1 System) using 20X objectives. Ki67 positive cells were counted using ImageJ software. Results were expressed as percentage of Ki67-positive cells in 5 visual fields of three independent experiments.

2.2.7 Western blot: Western blot was performed as previously described (32). Briefly, cells were lysed on ice for 30 minutes in RIPA Lysis and Extraction buffer (ThermoFisher Scientific). Heart tissue was harvested and homogenized with TissueLyser (Qiagen), 20 mg of tissue was shaken at 120 Hz for two repetitions of 2 minutes in the same buffer then leaved on ice for 30 minutes. Equal amounts of total proteins were separated on Mini-PROTEAN® TGX™ (Biorad) and transferred into nitrocellulose membranes using the Trans-Blot® Turbo system (Biorad). After the blocking step, the membranes were incubated overnight at 4 °C with the primary antibodies and then with secondary peroxidase-conjugated antibodies. For immunodetection, membranes were incubated with Clarity™ or Clarity™ Max Western ECL blotting substrates (Biorad), and the images were obtained with ChemiDoc camera (Biorad).

2.2.8 Reverse transcription (RT) - PCR: RNA was extracted using the RNeasy Mini Kit (Qiagen) and quantified with Nanodrop (ThermoFisher Scientific). RT-PCR was performed as previously described (33). Briefly, 500 ng of RNA were reverse transcribed using SuperScript™ First-Strand Synthesis System (ThermoFisher Scientific). The Real-time PCR experiments were conducted on the StepOne™ Real-Time PCR System using Perfecta SYBR Green SuperMix with ROX kit (Quanta Biosciences). The final concentration of all the primers was 500 nM. Primer sequences: *Rpl13a*: forward 5'-CCGCAAGATCCGCAGACGCA-3', reverse 5'-CTGATGGGACCGGACGCGG-3'; *Notch1*: forward 5'-GGTGCGAGCGCAGTGAAGGA-3', reverse 5'-CCCGCTGCTGCCCTCTTTCC-3'; *Hey1*: forward 5'-TCGTCCCAGGTTTTGGCCCG-3', reverse 5'-TCTAGCTTCGCAGATCCCTGCT-3'; *Hey2*: forward 5'-TTTCGCCGCGATGAAGCGCC-3', reverse 5'-TGAGCTTGCACTGTGCCCGGAG-3'; *Hes1*: forward 5'-ATTCCTCGTCCCCGGTGGCT-3', reverse 5'-TCTTGCCCGGCGCCTCTTCT-3'. Changes in gene expression were calculated by the $2^{-\Delta\Delta Ct}$ formula using *Rpl13a* as reference gene.

2.2.9 GFP-LC3 fluorescence: Autophagy was assessed by using green fluorescent protein (GFP)-tagged microtubule-associated protein light chain 3 (LC3) expressing cells. GFP-LC3 expression plasmid (0.8 µg) with plasmid encoding Notch1 (1.2 µg) or empty (pcDNA3 CTRL) were transfected using Lipofectamine LTX (ThermoFisher Scientific). H9c2 cells were treated with lapatinib 5 µM for 24h and then fixed with PFA 4% for 15 minutes. Fluorescence analysis was carried out on a confocal microscope (Nikon A1 System) using 60X objectives. Results were expressed as mean of the number of GFP-LC3 dots per cell counted in 3 visual fields of three independent experiments.

2.2.10 Cell cycle analysis: For cell cycle analysis, H9c2 were fixed in pre-cooled 70% ethanol for 30 minutes on ice, and subsequently washed with PBS 1X before being centrifuged. The resulting cell pellet was then resuspended in a PI staining solution consisting of 0.1% Triton X-100, 50 µg/mL PI, and 100 µg/mL RNAse A in PBS 1X, and incubated for 30 minutes at room temperature. Finally, PI fluorescence was measured using Attune Nxt Flow cytometer (ThermoFisher Scientific), and dates were analyzed with Attune Nxt Software (ThermoFisher Scientific).

2.2.11 Basal mitochondrial membrane potential: Cells were loaded with 20 nM tetramethylrhodamine methyl ester (TMRM) for 30 min at 37 °C. To obtain and analyze basal levels, cells were stimulated with 10 nM carbonyl cyanide p-trifluoromethoxyphenylhydrazone (FCCP), a strong uncoupler of oxidative phosphorylation. Image acquisitions were performed with a motorized Nikon AX R confocal microscope with a 40X/0.6 PlanApo objective and laser LU-N4S 405/488/561/640.

2.2.12 Mitochondrial reactive oxygen species (ROS) measurements: ROS measurements were performed according to (34). Briefly, measurement of mitochondrial superoxide ($mtO_2^{\bullet -}$) production was performed on cells incubated for 30 min at 37 °C in the presence of 5 μM mitoSOX red. The fluorescence was evaluated on Nikon AX R confocal microscope with a PlanApo 60X/1.4 objective and laser LU-N4S 405/488/561/640.

2.2.13 Primary neonatal mouse cardiomyocytes: Neonatal cardiac cells were harvested from 1-2 days-old C57BL/6 pups (IRCCS Ospedale Policlinico San Martino approval 792/2015-PR) and cultured with or without NRG-1 100 ng/ml and/or γ-secretase inhibitor MK-0752 (MK) 5 μM. Experiments were started 24h after seeding cells and cardiomyocyte proliferation was examined by counting cells co-stained for troponin T and Ki67.

2.2.14 ErbB2 transgenic mice: The study was performed in accordance with the Guide for the Care and Use of Laboratory Animals of the National Institutes of Health recommendations. The protocol was approved by the Animal Care and Use Committee of the Johns Hopkins Medical Institutions (Animal Welfare Assurance No. A-3273-01). The wild-type (WT) and transgenic (TG; ErbB2^{tg}) mice used in this study were developed as described previously (35). All the wild- type and transgenic mice were housed under a 12h light-dark cycle with free access to food and water. Expression of Notch1 and N1ICD was assessed in total heart lysates from 1-week-old and 2-week-old male animals.

2.2.15 mRNA microarray: Total RNA was isolated from the hearts of 3 months-old wild type and ErbB2^{tg} male mice (4 animals per group). Agilent G4122A mouse 44K microarray slides were used to analyze gene expression in cardiac tissue. These genes were analyzed by cluster analysis to delineate patterns of expression between the two groups. Differentially expressed genes (DEGs) were identified by log2 z-transformation followed by Significance Analysis of Microarray consisting of: statistical significance (z-test p value ≤ 0.05 with FDR ≤ 0.30) and absolute z ratio threshold ($|z\ ratio| \leq 1.5$); probe average z score signal for each pairwise comparisons ≥ 0; a sample group level one way ANOVA p-value ≤ 0.05 globally for sample group character quality; and probe detect p-value ≤ 0.01 to ensure good quality signal. Genes were assigned to Gene Ontology gene sets (MSigDB).

2.2.16 Statistical analysis: Results are expressed as mean ± SEM of at least 3 independent experiments. For comparisons between two groups, two-tailed unpaired Student's t test was used. When more than two groups were compared, one-way analysis of variance and multiple comparisons test was used.

3 RESULTS

3.1 ErbB2 is upstream of Notch1 activation in H9c2 cells

To investigate the possible regulation of Notch1 by ErbB2 in cardiomyocytes, we overexpressed ErbB2 by transfecting H9c2 cells with a plasmid containing the sequence of rat *ErbB2*. Overexpression of ErbB2 was confirmed by Western blot (Fig. 1A). H9c2 cells transfected with ErbB2 showed an increase of Notch1 intracellular domain (N1ICD), the active form of Notch1, compared to cells transfected with the empty vector (pcDNA3) (Fig. 1A). ErbB2 overexpression did not affect *Notch1* mRNA levels, suggesting that the effect of ErbB2 on Notch1 is post-transcriptional (Fig 1B). Conversely, we observed an increase in *Hey2 (*Hairy and Enhancer of Split with YRPW-2*)* expression and, although not statistically significant, a trend for an increase in the expression of the other Notch target genes *Hey1* and *Hes1* (Hairy and Enhancer of Split-1) (Fig. 1B). Since p38 activation increases N1ICD in RAS-transformed human cells (36), we investigated the possible role of p38 MAPK also in ErbB2-mediated Notch1 activation. First, we estimated the activation of p38, and found an increase in p38 phosphorylation in cells overexpressing ErbB2 compared to the cells transfected with the empty vector (Fig. 1A). To determine whether ErbB2 enhanced N1ICD formation through a p38-mediated mechanism, H9c2 cells were then treated for 24h with 10 μM SB203580, a p38 MAPK inhibitor, and N1ICD protein level was determined by Western blot. Cells overexpressing ErbB2 showed an increase of N1ICD, which was reduced by SB203580 (Fig. 1C). Additionally, to investigate whether other kinases are involved in ErbB2-mediated Notch1 activation, we evaluated the phosphorylation of AKT, p44/42 (also called ERK1/2) and SAPK/JNK in H9c2 overexpressing ErbB2 compared to cells transfected with the empty vector. ErbB2 overexpression determined an increase in SAPK/JNK phosphorylation, while phosphorylation of AKT and ERK1/2 remained unchanged (Supplementary Fig. S1A). To determine the role of JNK in ErbB2-mediated induction of N1ICD, H9c2 cells were treated for 24h with 100 μM SP600125, a JNK inhibitor, and N1ICD protein levels were determined by Western blot. The treatment with SP600125 induced N1ICD regardless of overexpression of ErbB2 (Supplementary Fig. S1B). Since SP600125 increases the phosphorylation of p38 MAPK (37), we hypothesized that the induction of N1ICD by SP600125 could be determined by activation of p38. To investigate this possibility, H9c2 cells were co-treated with SP600125 and SB203580, and N1ICD protein levels were determined by Western blot. We found that the SP600125-mediated increase in N1ICD was reduced by SB203580, confirming the role of p38 MAPK in Notch1 activation (Supplementary Fig. S1C). Taken together, these results suggest that ErbB2 induces Notch1 activation, at least in part, by a p38-dependent mechanism.

To gain further evidence that ErbB2 controls Notch1 activation in H9c2 cells, we used the opposite approach, i.e. we inhibited ErbB2 through incubation with lapatinib, a selective, reversible, ATP-competitive TKI that reduces ErbB2 phosphorylation (38). It is known that H9c2 cells express NRG-1 and ErbB2 (39), thus having a NRG-1-ErbB2 autocrine/paracrine axis. Cells were treated with two different concentrations of lapatinib (0.5 and 5 μM) for 24h, then we determined the effect of ErbB2 inhibition on Notch1 protein and transcript levels and Notch target gene expression. We found that treatment with lapatinib 0.5 μM and 5 μM for 24h significantly reduced the protein levels of Notch1 precursor (N1PC), Notch1 transmembrane (N1TM), and Notch1 intracellular domain (N1ICD) (Fig. 2A), as well as *Notch1* mRNA abundance (Fig.2B). Lapatinib also dose-dependently reduced the expression of Notch target genes, *Hey1* and *Hey2*, while the levels of *Hes1*, were lower, as compared with control, only after incubation with 5 μM lapatinib (Fig. 2B). We further investigated *Hes1* response by testing additional concentrations of lapatinib (1 μM and 2 μM). Supplementary Figure S2 shows a reduction in *Hes1* expression starting at 1 μM, indicating that, likely due to multiple pathways regulation (40), higher drug concentration is needed to affect *Hes1* mRNA compared to *Hey1* and *Hey2*.

3.2 ErbB2 and Notch1 control autophagic flux in H9c2 cells

Since inhibition of ErbB2 causes dysregulation of autophagy in cardiomyocytes (41) and Notch1 has also been shown to modulate autophagy, albeit in lymphocytes (42), we determined the levels of LC3-II and p62 in H9c2 cells in which the ErbB2 or Notch1 pathway were pharmacologically inhibited. When autophagy is activated, a cytosolic, cleaved, form of LC3 (LC3-I) is conjugated to phosphatidylethanolamine to form LC3-II, which is associated with autophagic vesicles; furthermore, p62, a ubiquitin-binding scaffold protein, delivers autophagy substrates to autophagosomes for degradation (43).

Treatment with lapatinib 0.5 μM and 5 μM increased the protein level of LC3-II compared with untreated cells in a dose-dependent manner (Fig. 3A). In addition, we observed an accumulation of p62 protein in H9c2 cells treated with lapatinib 5 μM for 24h (Fig. 3A). To determine whether the increase in LC3-II by lapatinib was due to autophagosome formation or accumulation of autophagosomes, we used bafilomycin A1 (BafA1) to suppress autophagic flux (44). H9c2 cells were treated with lapatinib 5 μM for 24h in the presence or absence of 100 nM BafA1 during the last 4h of the treatment with lapatinib. Both BafA1 and lapatinib 5 μM increased the level of LC3-II and p62, but BafA1 did not further increase protein levels of both LC3-II and p62 in lapatinib-treated cells, suggesting that treatment with lapatinib determined a suppression of autophagic flux (Fig. 3B). To confirm that the effects of lapatinib on Notch1 and autophagy are due to inhibition of ErbB2, we

treated H9c2 cells with CP-724714, a selective inhibitor of ErbB2 autophosphorylation. We found that, similar to lapatinib, treatment with CP-724714 at 5 μM and 10 μM for 24h significantly reduced N1ICD and induced LC3-II and p62 protein levels in a dose-dependent manner (Supplementary Fig. S3). To address the question of whether Notch1 regulates autophagy in H9c2 cells, we used DAPT, a γ-secretase inhibitor that blocks Notch1 activation. After 24 hour-incubation with 5 μM DAPT, N1ICD was significantly less than in control condition, as expected. Moreover, the levels of LC3-II and p62 protein were increased (Fig. 3C). Similar to what we observed with lapatinib, we did not observe differences in LC3-II and p62 protein levels between H9c2 cells treated with DAPT alone or DAPT along with 100 nM BafA1 during the last 4h of incubation, suggesting that inhibition of Notch1 activation led to autophagic flux blockade like inhibition of ErbB2 (Fig. 3D).

3.3 Notch1 overexpression rescues the autophagic flux impaired by lapatinib treatment in H9c2 cells

Building upon the evidence that ErbB2 is upstream of Notch1 and that both ErbB2 and Notch1 inhibition results in stalled autophagy in H9c2 cells, we hypothesized that forced activation of Notch1 would counteract the blockade of autophagic flux induced by lapatinib. To prove this, H9c2 cells were transfected with a plasmid containing the sequence of N1ICD or with an empty vector (pcDNA3), treated with lapatinib 5 μM, and evaluated for autophagy. Overexpression of N1ICD was confirmed by Western blot analysis (Fig. 4A). Upon treatment with lapatinib 5 μM for 24h, H9c2 cells overexpressing N1ICD showed reduced accumulation of LC3-II and p62 proteins, compared with cells transfected with the empty vector (Fig. 4A). Autophagic flux was investigated also by using a plasmid expressing GFP-LC3 (45). H9c2 cells were transfected with a vector expressing GFP-LC3 in the presence or absence of the N1ICD-containing plasmid and then treated with lapatinib 5 μM for 24h. Confocal microscopy images showed that lapatinib significantly increased the number of autophagosomes, represented by green puncta structures, compared to control untreated cells, and N1ICD overexpression counteracted this effect (Fig. 4B). To assess the impact of autophagy blockade on mitochondria, we treated H9c2 cells with 5 μM lapatinib for 24h and measured mitochondrial membrane potential (Δψm) and mitochondrial ROS (mtROS) levels. We observed an increase in both Δψm and mtROS, and N1ICD overexpression attenuated the increase in Δψm but not mtROS production (Supplementary Fig. S4A and B). These results support the hypothesis that Notch1 is involved in ErbB2-driven stall of the autophagic flux in H9c2 cells.

3.4 Block of autophagic flux by treatment with lapatinib is associated with proliferation, but not with apoptosis or senescence of H9c2 cells

To investigate the functional effects of lapatinib-induced block of autophagic flux, we assessed cell proliferation, apoptosis, and senescence. The number of H9c2 cells decreased after treatment with 5 μM lapatinib starting from 48h of treatment (Fig. 5A). Flow cytometric analysis did not reveal an increase in apoptosis in H9c2 cells treated with lapatinib 5 μM for 24, 48 and 72 hours (Fig. 5B). The proportion of senescent cells, under the experimental conditions used, was low and remained unchanged following up to 72-hours exposure to lapatinib, as compared with control (Fig. 5C). Thus, we concluded that the reduction in live cells upon prolonged treatment with lapatinib was secondary to inhibition of proliferation, rather than to apoptosis or senescence.

3.5 Notch1 overexpression counteracts lapatinib-caused reduction of proliferation of H9c2 cells

To determine whether overexpression of N1ICD, which restores the autophagic flux, could also reverse the negative impact of lapatinib on cell proliferation, we transfected H9c2 cells with N1ICD or an empty vector. Re-expression of N1ICD counteracted the reduction of cell proliferation caused by lapatinib after 72h of treatment (Fig. 6A).

As expected, and consistent with data shown in Fig 5B, overexpression of N1ICD did not affect apoptosis or senescence, either in the presence or absence of lapatinib (Supplementary Fig. S5 and S6). Treatment with lapatinib 5 μM for 24 and 48 hours, either with or without N1ICD overexpression, did not significantly modulate the levels of caspase-3 full-length (FL) and cleaved forms, and Bax or Bcl-2 proteins (Supplementary Fig. S5B). Similarly, no differences were observed in the number of SA-β-gal-positive H9c2 cells after the treatment with 5 μM lapatinib for 48 or 72 hours, with or without the overexpression of N1ICD (Supplementary Fig. S6).

We further investigated the mechanism by which ectopic N1ICD expression counteracts the effects of lapatinib on cell proliferation by analyzing the expression of the nuclear protein Ki67, which is present exclusively in proliferating cells (46). Treatment with lapatinib 5 μM for 24, 48 and 72 hours reduced the percentage of Ki67 positive (Ki67+) cells and overexpression of N1ICD prevented this reduction (Fig. 6B). Consistently, treatment with lapatinib 5 μM for 48 and 72 hours increased cell population in G0/G1 - phase and reduced percentage of cells in S/G2/M phase. H9c2 cells overexpressing N1ICD exhibited a trend towards a decreased percentage of the cell population in G0/G1 and an increased percentage in S/G2/M (Supplementary Fig. S7). These results indicate that active Notch1 counteracts lapatinib-induced reduction of cell proliferation by promoting cell cycle progression.

3.6 ErbB2 controls Notch1 activation in primary mouse cardiomyocytes and in vivo

To confirm the data obtained with H9c2 cells, primary mouse neonatal cardiomyocytes were treated with NRG-1 to activate ErbB2 signaling, with or without the γ-secretase inhibitor MK-0752 (MK) at

a concentration of 5 μM. Proliferation of cardiomyocytes was assessed by counting the number of Ki67/troponin T double positive cells. As shown in Fig. 7A, exogenous NRG-1 significantly increased cell proliferation and this effect was antagonized by inhibition of γ-secretase and, thereby, Notch1 activation. Thus, Notch1 mediates ErbB2-dependent proliferation in primary mouse cardiomyocytes like it does in the H9c2 cell line. Furthermore, the hearts of ErbB2^{tg} mice were characterized by increased N1ICD protein levels as compared with wild type littermates, while N1TM was not modulated (Fig. 7B).

Next, we performed microarray analysis on the RNA extracted from hearts of wild-type and ErbB2^{tg} mice. In total, we identified 2494 DEGs. We selected a panel of 184 genes related to Notch signaling based on Mouse Molecular Signatures Database (MSigDB, https://www.gsea-msigdb.org/gsea/msigdb/index.jsp) and found that 100 of them were expressed and detected in our array, highlighting the importance of Notch in the heart. Among the 100 genes related to Notch signaling, 58 were differentially expressed between ErbB2^{tg} and wild-type mice, confirming ErbB2-mediated regulation of Notch in the heart (Supplementary Fig. S8 and Tables 1 and 2). Among the receptors and ligands of Notch, we found that *Jagged1* and *Jagged2* were upregulated, while *Notch3* was downregulated in ErbB2^{tg} vs wild type mice. Other Notch pathway components expressed in cardiomyocytes, *Notch1*, *4* and *Dll1*, *Dll4*, were not differently expressed in ErbB2^{tg} mice compared to wild-type littermates. Among the top ten genes exhibiting the most pronounced differences *Mmp14*, *Tmem100*, *Tgfb2*, *App*, *Hes1*, and *Sox9* were upregulated, while *Pgam2*, *Notch3*, *Rcan2*, and *Epn1* were downregulated in ErbB2^{tg} mice.

4 DISCUSSION

In this study, we explored the interplay between ErbB2 and Notch1 pathways in H9c2 cardiomyoblasts and cardiomyocytes using both pharmacological and gene overexpression methods. Our findings reveal that overexpression of ErbB2 activates Notch1, partly through a p38-dependent mechanism, while inhibition of ErbB2 with lapatinib decreases Notch1 activation. Furthermore, we observed that the inhibition of autophagic flux and proliferation induced by lapatinib in H9c2 cardiomyoblasts could be reversed by overexpressing active Notch1. Additionally, we found that the proliferation of primary neonatal mouse cardiomyocytes in response to NRG-1 was hindered when Notch1 activation was inhibited.

The Notch pathway is evolutionarily conserved, as expected for a pathway which is a major player in determining cell fate during development and in postnatal life, particularly in continuously renewing tissues where Notch controls cell stemness, differentiation, and survival. Given this role, it is not

surprising that Notch is intricately intertwined with other major pathways involved in these biological processes (47). The crosstalk between Notch and ErbB2/HER2 has been investigated thoroughly in cancer cells, where these pathways interact to modulate cell proliferation and survival (48). In particular, in HER2 positive breast cancer, Notch1 is activated following the inhibition of ErbB2 by trastuzumab or lapatinib, contributing to resistance to both treatments (18, 49, 50). One proposed mechanism for this activation is the enhanced membrane expression of the Notch ligand Jagged1 (51). However, while these studies implicate an inhibitory action of ErbB2 on Notch1, other studies have reported induction of Notch1 signaling by ErbB2 activation in breast cancer (20).

Here we show, for the first time, that ErbB2 and Notch1 interact in H9c2 cardiomyoblasts, in which Notch1 activation is stimulated by overexpression and blunted by inhibition of ErbB2. Moreover, we provide cues of enhanced Notch1 activation in the hearts of mice with cardiac-restricted overexpression of ErbB2, showing differential expression of approximately 50 genes related to Notch signaling, including *Hes1*, *Mmp14* (52), *Tmem100* (53), *Tgf-β2* (54), and *Sox9* (55). Our data are consistent with previous studies showing that Notch1 is involved in the response to physiological recruitment of ErbB2 by NRG-1. Specifically, in zebrafish, Notch signaling is activated by ErbB2 in cardiomyocytes to direct ventricular chamber morphogenesis and, in turn, Notch signaling cell-autonomously inhibits ErbB2 signaling (56). In addition, in mice, Notch1 regulates cardiac morphogenesis through EphrinB2- and Hand2- mediated expression of NRG-1 (57, 56).

Consistently with previous studies in human fibroblasts showing that Notch1 signaling is activated by oncogenic Ras through a p38-mediated pathway (36) we found that, in H9c2, ErbB2-mediated phosphorylation is required to increase the levels of N1ICD. The mechanisms of p38-mediated activation of Notch1 remain to be determined; it may be related to increased mRNA stability (58) or to phosphorylation of presenilin and/or nicastrin, two components of the γ-secretase complex (59). On the other hand, Notch ligands Jagged1 and Jagged2 were found upregulated in the hearts of ErbB2^{tg} mice, hence ligand-mediated activation of Notch1 by ErbB2 is also possible. It should be mentioned that other ErbB2 downstream players such as GSK3β/β-catenin or YAP can potentially regulate Notch. Specifically, in neonatal cardiomyocytes ErbB2 inhibits GSK3β and enhances the expression level of β-catenin (60) that could activate Notch signaling (61). Similarly, ErbB2 signaling has been shown to lead to phosphorylation of YAP (62) which, in turn, acts upstream of Notch signaling (63). Further studies are needed to investigate the involvement of these pathways in ErbB2-mediated Notch1 activation.

Recent studies have shown that Notch regulates autophagy in various context: cancer cells (64), in the brain following a hypoxic–ischemic injury (65), in the heart in the presence of oxygen and glucose

deprivation-induced myocardial damage (66), and in T cells (42). Conversely, autophagy-mediated Notch inhibition impacts stem cell differentiation (67), including differentiation of cardiac cells (68) and interferes with cancer cell metastasis (69). Here, we report that Notch1 inhibition by a γ-secretase inhibitor blocks the autophagic flux in H9c2 cells similarly to lapatinib-mediated ErbB2 inhibition. In addition, we found that transient overexpression of N1ICD counteracted the stall of autophagy induced by lapatinib, indicating that, in H9c2, Notch1 modulates autophagy downstream of ErbB2. Importantly, we observed that ErbB2 inhibition also alters mitochondrial metabolism, as reflected by the increase of the mitochondria membrane potential and mitochondrial ROS production. Our findings align with previous research describing the block of autophagic flux and accumulation of damaged mitochondria following ErbB2 inhibition by trastuzumab (11). However, while N1ICD overexpression counteracted the alteration of mitochondrial potential, it did not prevent the increase in mitochondrial ROS production, indicating that lapatinib impairs mitochondria metabolism also by other, Notch1-independent, mechanisms.

Autophagy is an evolutionarily conserved process that plays a crucial role in regulating cardiac homeostasis (70) and dysregulation of autophagy in cardiomyocytes has been implicated in the pathogenesis of a wide range of cardiac diseases, including cardiomyopathy and HF (71, 72). Several studies suggest that tight regulation of the autophagic process in the heart is necessary because excessive activation or, conversely, blockade of autophagic flux can be detrimental. In particular, a complex relationship exists between autophagy blockade and cell survival and growth (73) and, depending on the cell context, autophagy blockade can lead to increased cell death, as damaged cellular components are not cleared away and can accumulate to toxic levels (74), or promotes cell survival, by preventing the breakdown of critical cellular components and preserving energy reserves (75). Similarly, autophagy blockade can lead to reduced cell growth, as the cell is unable to break down and recycle cellular components for energy or biosynthesis, but also to increased cell growth (76). We found that blockade of the autophagic flux by ErbB2 or Notch1 inhibition was associated with decreased proliferation of H9c2 cells and that the ectopic expression of N1ICD in lapatinib-treated cells restored proliferation. These data linking Notch to cardiac cells proliferation are consistent with those from other authors, who showed that Notch1 promotes proliferation of cardiac progenitor cells (77) and immature cardiomyocytes (23), and induces cell cycle re-entry in quiescent cardiomyocytes (78, 23). The knowledge of the mechanisms regulating cardiac cell proliferation is crucial since adult cardiomyocytes have limited renewal capacity, inadequate for restoring the damaged heart, but that could be promoted, thus stimulating the intrinsic cardiac regenerative potential, as reported by several authors (60, 79-81).

The findings of our study expand the existing knowledge on the roles of ErbB2 and Notch1 in cardiac biology and may have translational implications when considering the cardiotoxicity of HER2-directed antitumor therapies. Although the Notch signaling pathway undergoes gradual attenuation in the postnatal heart, it can be reactivated in the adult myocardium following ischemic injury (24, 25, 82), hypertrophy (83) or HF (84), thereby reducing apoptosis and pathological hypertrophy of cardiomyocytes (83, 25) as well as fibrosis (85). Since Notch1 is central to the cardiac response to injury (20, 47), in principle, part of the cardiotoxicity of HER2 targeting drugs might lie in the inhibition of Notch1 activation, leading to impaired adaptation of the heart to various stresses.

In conclusion, our experiments show that ErbB2 is upstream of Notch1 activation in H9c2 cardiomyoblasts and in primary neonatal mouse cardiomyocytes, and that Notch1 inhibition or activation mediates at least some effects of ErbB2 inhibition or stimulation, respectively. We acknowledge that most of our findings were obtained in H9c2 cardiomyoblasts, which have similarities but also important differences with cardiomyocytes. For instance, cardiomyoblasts derived from the embryonic rat heart have higher expression of ErbB2 than adult mature cardiomyocytes (7). Nonetheless, primary cultures of cardiomyocytes include a certain number of non-cardiomyocytes and display temporal changes in the expression of Notch receptors and Notch ligands, which make assessments such as the ones made here difficult (23). Moreover, overexpression experiments in primary cultures are technically challenging. It is noteworthy that we collected confirmatory results with primary neonatal mouse cardiomyocytes and whole mouse hearts, suggesting that the crosstalk between ErbB2 and Notch1 does occur *in vivo*. Further work is needed to consolidate these findings and evaluate whether cardiac Notch1 preservation/activation may protect against the adverse effects of anti-HER2 medications in the heart.

References

[1] O. Martínez-Sáez, A. Prat (2021) Current and Future Management of HER2-Positive Metastatic Breast Cancer. JCO Oncol Pract 17:594-604.

[2] B. Wadugu, B. Kühn (2012) The role of neuregulin/ErbB2/ErbB4 signaling in the heart with special focus on effects on cardiomyocyte proliferation. Am J Physiol Heart Circ Physiol 302:H2139-2147.

[3] L. P. Grazette, W. Boecker, T. Matsui, M. Semigran, T. L. Force, R. J. Hajjar, A. Rosenzweig (2004) Inhibition of ErbB2 causes mitochondrial dysfunction in cardiomyocytes: implications for herceptin-induced cardiomyopathy. J Am Coll Cardiol 44:2231-2238.

[4] L. I. Gordon, M. A. Burke, A. T. Singh, S. Prachand, E. D. Lieberman, L. Sun, T. J. Naik, S. V. Prasad, H. Ardehali (2009) Blockade of the erbB2 receptor induces cardiomyocyte death through mitochondrial and reactive oxygen species-dependent pathways. J Biol Chem 284:2080-2087.

[5] B. M. Necela, B. C. Axenfeld, D. J. Serie, J. M. Kachergus, E. A. Perez, E. A. Thompson, N. Norton (2017) The antineoplastic drug, trastuzumab, dysregulates metabolism in iPSC-derived cardiomyocytes. Clin Transl Med 6:5.

[6] S. Rohrbach, U. Muller-Werdan, K. Werdan, S. Koch, N. F. Gellerich, J. Holtz (2005) Apoptosis-modulating interaction of the neuregulin/erbB pathway with anthracyclines in regulating Bcl-xS and Bcl-xL in cardiomyocytes. J Mol Cell Cardiol 38:485-493.

[7] C. De Lorenzo, R. Paciello, G. Riccio, D. Rea, A. Barbieri, C. Coppola, N. Maurea (2018) Cardiotoxic effects of the novel approved anti-ErbB2 agents and reverse cardioprotective effects of ranolazine. Onco Targets Ther 11:2241-2250.

[8] F. Timolati, D. Ott, L. Pentassuglia, M. N. Giraud, J. C. Perriard, T. M. Suter, C. Zuppinger (2006) Neuregulin-1 beta attenuates doxorubicin-induced alterations of excitation-contraction coupling and reduces oxidative stress in adult rat cardiomyocytes. J Mol Cell Cardiol 41:845-854.

[9] F. Belmonte, S. Das, P. Sysa-Shah, V. Sivakumaran, B. Stanley, X. Guo, N. Paolocci, M. A. Aon, M. Nagane, P. Kuppusamy, C. Steenbergen, K. Gabrielson (2015) ErbB2 overexpression upregulates antioxidant enzymes, reduces basal levels of reactive oxygen species, and protects against doxorubicin cardiotoxicity. Am J Physiol Heart Circ Physiol 309:H1271-1280.

[10] F. Jacob, A. Y. Yonis, F. Cuello, P. Luther, T. Schulze, A. Eder, T. Streichert, I. Mannhardt, M. N. Hirt, S. Schaaf, J. Stenzig, T. Force, T. Eschenhagen, A. Hansen (2016) Analysis of Tyrosine Kinase Inhibitor-Mediated Decline in Contractile Force in Rat Engineered Heart Tissue. PLoS One 11:e0145937.

[11] N. Mohan, Y. Shen, Y. Endo, M. K. ElZarrad, W. J. Wu (2016) Trastuzumab, but Not Pertuzumab, Dysregulates HER2 Signaling to Mediate Inhibition of Autophagy and Increase in Reactive Oxygen Species Production in Human Cardiomyocytes. Mol Cancer Ther 15:1321-1331.

[12] D. J. Slamon, G. M. Clark, S. G. Wong, W. J. Levin, A. Ullrich, W. L. McGuire (1987) Human breast cancer: correlation of relapse and survival with amplification of the HER-2/neu oncogene. Science 235:177-182.

[13] B. T. Nemeth, Z. V. Varga, W. J. Wu, P. Pacher (2017) Trastuzumab cardiotoxicity: from clinical trials to experimental studies. Br J Pharmacol 174:3727-3748.

[14] A. Denegri, T. Moccetti, M. Moccetti, P. Spallarossa, C. Brunelli, P. Ameri (2016) Cardiac toxicity of trastuzumab in elderly patients with breast cancer. J Geriatr Cardiol 13:355-363.

[15] G. W. De Keulenaer, K. Doggen, K. Lemmens (2010) The vulnerability of the heart as a pluricellular paracrine organ: lessons from unexpected triggers of heart failure in targeted ErbB2 anticancer therapy. Circ Res 106:35-46.

[16] T. Kitani, S. G. Ong, C. K. Lam, J. W. Rhee, J. Z. Zhang, A. Oikonomopoulos, N. Ma, L. Tian, J. Lee, M. L. Telli, R. M. Witteles, A. Sharma, N. Sayed, J. C. Wu (2019) Human-Induced Pluripotent Stem Cell Model of Trastuzumab-Induced Cardiac Dysfunction in Patients With Breast Cancer. Circulation 139:2451-2465.

[17] J. Lindsay, X. Jiao, T. Sakamaki, M. C. Casimiro, L. A. Shirley, T. H. Tran, X. Ju, M. Liu, Z. Li, C. Wang, S. Katiyar, M. Rao, K. G. Allen, R. I. Glazer, C. Ge, P. Stanley, M. P. Lisanti, H. Rui, R. G. Pestell (2008) ErbB2 induces Notch1 activity and function in breast cancer cells. Clin Transl Sci 1:107-115.

[18] C. Osipo, P. Patel, P. Rizzo, A. G. Clementz, L. Hao, T. E. Golde, L. Miele (2008) ErbB-2 inhibition activates Notch-1 and sensitizes breast cancer cells to a gamma-secretase inhibitor. Oncogene 27:5019-5032.

[19] L. Marracino, F. Fortini, E. Bouhamida, F. Camponogara, P. Severi, E. Mazzoni, S. Patergnani, E. D'Aniello, R. Campana, P. Pinton, F. Martini, M. Tognon, G. Campo, R. Ferrari, F. Vieceli Dalla Sega, P. Rizzo (2021) Adding a "Notch" to Cardiovascular Disease Therapeutics: A MicroRNA-Based Approach. Front Cell Dev Biol 9:695114.
[20] R. Ferrari, P. Rizzo (2014) The Notch pathway: a novel target for myocardial remodelling therapy? Eur Heart J 35:2140-2145.
[21] X. L. Zhou, X. Wu, Q. R. Xu, R. R. Zhu, H. Xu, Y. Y. Li, S. Liu, H. Huang, X. Xu, L. Wan, Q. C. Wu, J. C. Liu (2019) Notch1 provides myocardial protection by improving mitochondrial quality control. J Cell Physiol 234:11835-11841.
[22] H. Pei, X. Song, C. Peng, Y. Tan, Y. Li, X. Li, S. Ma, Q. Wang, R. Huang, D. Yang, D. Li, E. Gao, Y. Yang (2015) TNF-α inhibitor protects against myocardial ischemia/reperfusion injury via Notch1-mediated suppression of oxidative/nitrative stress. Free Radic Biol Med 82:114-121.
[23] C. Collesi, L. Zentilin, G. Sinagra, M. Giacca (2008) Notch1 signaling stimulates proliferation of immature cardiomyocytes. J Cell Biol 183:117-128.
[24] N. A. Gude, G. Emmanuel, W. Wu, C. T. Cottage, K. Fischer, P. Quijada, J. A. Muraski, R. Alvarez, M. Rubio, E. Schaefer, M. A. Sussman (2008) Activation of Notch-mediated protective signaling in the myocardium. Circ Res 102:1025-1035.
[25] P. Kratsios, C. Catela, E. Salimova, M. Huth, V. Berno, N. Rosenthal, F. Mourkioti (2010) Distinct roles for cell-autonomous Notch signaling in cardiomyocytes of the embryonic and adult heart. Circ Res 106:559-572.
[26] X. L. Zhou, L. Wan, Q. R. Xu, Y. Zhao, J. C. Liu (2013) Notch signaling activation contributes to cardioprotection provided by ischemic preconditioning and postconditioning. J Transl Med 11:251.
[27] B. Yu, B. Song (2014) Notch 1 signalling inhibits cardiomyocyte apoptosis in ischaemic postconditioning. Heart Lung Circ 23:152-158.
[28] S. Nistri, C. Sassoli, D. Bani (2017) Notch Signaling in Ischemic Damage and Fibrosis: Evidence and Clues from the Heart. Front Pharmacol 8:187.
[29] C. Fedele, G. Riccio, A. E. Malara, G. D'Alessio, C. De Lorenzo (2012) Mechanisms of cardiotoxicity associated with ErbB2 inhibitors. Breast Cancer Res Treat 134:595-602.
[30] H. A. Burris, C. W. Taylor, S. F. Jones, K. M. Koch, M. J. Versola, N. Arya, R. A. Fleming, D. A. Smith, L. Pandite, N. Spector, G. Wilding (2009) A phase I and pharmacokinetic study of oral lapatinib administered once or twice daily in patients with solid malignancies. Clin Cancer Res 15:6702-6708.
[31] F. Vieceli Dalla Sega, F. Fortini, D. Licastro, S. D. Monego, M. Degasperi, A. Ascierto, L. Marracino, P. Severi, M. D'Accolti, I. Soffritti, M. Brambilla, M. Camera, E. Tremoli, M. Contoli, S. Spadaro, G. Campo, R. Ferrari, E. Caselli, P. Rizzo (2024) Serum from COVID-19 patients promotes endothelial cell dysfunction through protease-activated receptor 2. Inflamm Res 73:117-130.
[32] F. Vieceli Dalla Sega, R. Mastrocola, G. Aquila, F. Fortini, C. Fornelli, A. Zotta, A. S. Cento, A. Perrelli, E. Boda, A. Pannuti, S. Marchi, P. Pinton, R. Ferrari, P. Rizzo, S. F. Retta (2019) KRIT1 Deficiency Promotes Aortic Endothelial Dysfunction. Int J Mol Sci 20.
[33] F. Vieceli Dalla Sega, D. Palumbo, F. Fortini, Y. D'Agostino, P. Cimaglia, L. Marracino, P. Severi, O. Strianese, R. Tarallo, G. Nassa, G. Giurato, G. Pecoraro, S. Caglioni, E. Mikus, A. Albertini, G. Campo, R. Ferrari, P. Rizzo, A. Weisz, F. Rizzo (2022) Transcriptomic profiling of calcified aortic valves in clonal hematopoiesis of indeterminate potential carriers. Sci Rep 12:20400.
[34] A. Wojtala, M. Bonora, D. Malinska, P. Pinton, J. Duszynski, M. R. Wieckowski (2014) Methods to monitor ROS production by fluorescence microscopy and fluorometry. Methods Enzymol 542:243-262.
[35] P. Sysa-Shah, Y. Xu, X. Guo, F. Belmonte, B. Kang, D. Bedja, S. Pin, N. Tsuchiya, K. Gabrielson (2012) Cardiac-specific over-expression of epidermal growth factor receptor 2 (ErbB2) induces pro-survival pathways and hypertrophic cardiomyopathy in mice. PLoS One 7:e42805.
[36] S. Weijzen, P. Rizzo, M. Braid, R. Vaishnav, S. M. Jonkheer, A. Zlobin, B. A. Osborne, S. Gottipati, J. C. Aster, W. C. Hahn, M. Rudolf, K. Siziopikou, W. M. Kast, L. Miele (2002) Activation of Notch-1 signaling maintains the neoplastic phenotype in human Ras-transformed cells. Nat Med 8:979-986.
[37] D. Vaishnav, P. Jambal, J. E. Reusch, S. Pugazhenthi (2003) SP600125, an inhibitor of c-jun N-terminal kinase, activates CREB by a p38 MAPK-mediated pathway. Biochem Biophys Res Commun 307:855-860.

[38] K. Leemasawat, A. Phrommintikul, S. C. Chattipakorn, N. Chattipakorn (2020) Mechanisms and potential interventions associated with the cardiotoxicity of ErbB2-targeted drugs: Insights from in vitro, in vivo, and clinical studies in breast cancer patients. Cell Mol Life Sci 77:1571-1589.
[39] M. Morano, C. Angotti, F. Tullio, G. Gambarotta, C. Penna, P. Pagliaro, S. Geuna (2017) Myocardial ischemia/reperfusion upregulates the transcription of the Neuregulin1 receptor ErbB3, but only postconditioning preserves protein translation: Role in oxidative stress. Int J Cardiol 233:73-79.
[40] C. L. Curry, L. L. Reed, B. J. Nickoloff, L. Miele, K. E. Foreman (2006) Notch-independent regulation of Hes-1 expression by c-Jun N-terminal kinase signaling in human endothelial cells. Lab Invest 86:842-852.
[41] N. Mohan, J. Jiang, W. J. Wu (2017) Implications of Autophagy and Oxidative Stress in Trastuzumab-Mediated Cardiac Toxicities. Austin Pharmacol Pharm 2.
[42] N. Marcel, A. Sarin (2016) Notch1 regulated autophagy controls survival and suppressor activity of activated murine T-regulatory cells. Elife 5.
[43] S. R. Yoshii, N. Mizushima (2017) Monitoring and Measuring Autophagy. Int J Mol Sci 18.
[44] D. J. Klionsky, F. C. Abdalla, H. Abeliovich, R. T. Abraham, A. Acevedo-Arozena, K. Adeli, L. Agholme, M. Agnello, P. Agostinis, J. A. Aguirre-Ghiso, H. J. Ahn, O. Ait-Mohamed, S. Ait-Si-Ali, T. Akematsu, S. Akira, H. M. Al-Younes, M. A. Al-Zeer, M. L. Albert, R. L. Albin, ..., B. Zuckerbraun (2012) Guidelines for the use and interpretation of assays for monitoring autophagy. Autophagy 8:445-544.
[45] G. Morciano, S. Patergnani, G. Pedriali, P. Cimaglia, E. Mikus, S. Calvi, A. Albertini, C. Giorgi, G. Campo, R. Ferrari, P. Pinton (2022) Impairment of mitophagy and autophagy accompanies calcific aortic valve stenosis favouring cell death and the severity of disease. Cardiovasc Res 118:2548-2559.
[46] J. Gerdes, H. Lemke, H. Baisch, H. H. Wacker, U. Schwab, H. Stein (1984) Cell cycle analysis of a cell proliferation-associated human nuclear antigen defined by the monoclonal antibody Ki-67. J Immunol 133:1710-1715.
[47] G. Aquila, A. Kostina, F. Vieceli Dalla Sega, E. Shlyakhto, A. Kostareva, L. Marracino, R. Ferrari, P. Rizzo, A. Malaschicheva (2019) The Notch pathway: a novel therapeutic target for cardiovascular diseases? Expert Opin Ther Targets 23:695-710.
[48] K. Zhang, P. Wong, C. Salvaggio, A. Salhi, I. Osman, B. Bedogni (2016) Synchronized Targeting of Notch and ERBB Signaling Suppresses Melanoma Tumor Growth through Inhibition of Notch1 and ERBB3. J Invest Dermatol 136:464-472.
[49] K. Pandya, K. Meeke, A. G. Clementz, A. Rogowski, J. Roberts, L. Miele, K. S. Albain, C. Osipo (2011) Targeting both Notch and ErbB-2 signalling pathways is required for prevention of ErbB-2-positive breast tumour recurrence. Br J Cancer 105:796-806.
[50] A. T. Baker, A. Zlobin, C. Osipo (2014) Notch-EGFR/HER2 Bidirectional Crosstalk in Breast Cancer. Front Oncol 4:360.
[51] D. Shah, D. Wyatt, A. T. Baker, P. Simms, D. S. Peiffer, M. Fernandez, E. Rakha, A. Green, A. Filipovic, L. Miele, C. Osipo (2018) Inhibition of HER2 Increases JAGGED1-dependent Breast Cancer Stem Cells: Role for Membrane JAGGED1. Clin Cancer Res 24:4566-4578.
[52] J. H. Chang, Y. H. Huang, C. M. Cunningham, K. Y. Han, M. Chang, M. Seiki, Z. Zhou, D. T. Azar (2016) Matrix metalloproteinase 14 modulates signal transduction and angiogenesis in the cornea. Surv Ophthalmol 61:478-497.
[53] E. H. Moon, Y. H. Kim, P. N. Vu, H. Yoo, K. Hong, Y. J. Lee, S. P. Oh (2020) TMEM100 is a key factor for specification of lymphatic endothelial progenitors. Angiogenesis 23:339-355.
[54] M. Klüppel, J. L. Wrana (2005) Turning it up a Notch: cross-talk between TGF beta and Notch signaling. Bioessays 27:115-118.
[55] A. Kohn, T. P. Rutkowski, Z. Liu, A. J. Mirando, M. J. Zuscik, R. J. O'Keefe, M. J. Hilton (2015) Notch signaling controls chondrocyte hypertrophy via indirect regulation of Sox9. Bone Res 3:15021.
[56] P. Han, J. Bloomekatz, J. Ren, R. Zhang, J. D. Grinstein, L. Zhao, C. G. Burns, C. E. Burns, R. M. Anderson, N. C. Chi (2016) Coordinating cardiomyocyte interactions to direct ventricular chamber morphogenesis. Nature 534:700-704.
[57] N. J. VanDusen, J. Casanovas, J. W. Vincentz, B. A. Firulli, M. Osterwalder, J. Lopez-Rios, R. Zeller, B. Zhou, J. Grego-Bessa, J. L. De La Pompa, W. Shou, A. B. Firulli (2014) Hand2 is an essential regulator for two Notch-dependent functions within the embryonic endocardium. Cell Rep 9:2071-2083.

[58] S. B. Frank, P. L. Berger, M. Ljungman, C. K. Miranti (2017) Human prostate luminal cell differentiation requires NOTCH3 induction by p38-MAPK and MYC. J Cell Sci 130:1952-1964.
[59] L. H. Kuo, M. K. Hu, W. M. Hsu, Y. T. Tung, B. J. Wang, W. W. Tsai, C. T. Yen, Y. F. Liao (2008) Tumor necrosis factor-alpha-elicited stimulation of gamma-secretase is mediated by c-Jun N-terminal kinase-dependent phosphorylation of presenilin and nicastrin. Mol Biol Cell 19:4201-4212.
[60] G. D'Uva, A. Aharonov, M. Lauriola, D. Kain, Y. Yahalom-Ronen, S. Carvalho, K. Weisinger, E. Bassat, D. Rajchman, O. Yifa, M. Lysenko, T. Konfino, J. Hegesh, O. Brenner, M. Neeman, Y. Yarden, J. Leor, R. Sarig, R. P. Harvey, E. Tzahor (2015) ERBB2 triggers mammalian heart regeneration by promoting cardiomyocyte dedifferentiation and proliferation. Nat Cell Biol 17:627-638.
[61] L. Zheng, S. D. Conner (2018) Glycogen synthase kinase 3β inhibition enhances Notch1 recycling. Mol Biol Cell 29:389-395.
[62] A. Aharonov, A. Shakked, K. B. Umansky, A. Savidor, A. Genzelinakh, D. Kain, D. Lendengolts, O. Y. Revach, Y. Morikawa, J. Dong, Y. Levin, B. Geiger, J. F. Martin, E. Tzahor (2020) ERBB2 drives YAP activation and EMT-like processes during cardiac regeneration. Nat Cell Biol 22:1346-1356.
[63] C. Engel-Pizcueta, C. Pujades (2021) Interplay Between Notch and YAP/TAZ Pathways in the Regulation of Cell Fate During Embryo Development. Front Cell Dev Biol 9:711531.
[64] A. Das, M. K. Narayanam, S. Paul, P. Mukhnerjee, S. Ghosh, D. G. Dastidar, S. Chakrabarty, A. Ganguli, B. Basu, M. Pal, U. Chatterji, S. K. Banerjee, P. Karmakar, D. Kumar, G. Chakrabarti (2019) A novel triazole, NMK-T-057, induces autophagic cell death in breast cancer cells by inhibiting γ-secretase-mediated activation of Notch signaling. J Biol Chem 294:6733-6750.
[65] K. Li, M. Lu, M. Cui, X. Wang, Y. Zheng (2023) The Notch pathway regulates autophagy after hypoxic-ischemic injury and affects synaptic plasticity. Brain Struct Funct 228:985-996.
[66] L. Y. Kong, Z. Xi, W. T. Ma, F. Y. Yang, L. D. Niu, J. H. Shi (2019) [Effects of Notch signal on the expressions of HIF-α and autophagy- related genes Beclin1, LC3I, LC3II in oxygen-glucose deprivation induced myocardial cell injury]. Zhongguo Ying Yong Sheng Li Xue Za Zhi 35:165-168.
[67] X. Wu, A. Fleming, T. Ricketts, M. Pavel, H. Virgin, F. M. Menzies, D. C. Rubinsztein (2016) Autophagy regulates Notch degradation and modulates stem cell development and neurogenesis. Nat Commun 7:10533.
[68] Z. Jia, J. Wang, W. Wang, Y. Tian, W. XiangWei, P. Chen, K. Ma, C. Zhou (2014) Autophagy eliminates cytoplasmic β-catenin and NICD to promote the cardiac differentiation of P19CL6 cells. Cell Signal 26:2299-2305.
[69] S. Zada, J. S. Hwang, T. H. Lai, T. M. Pham, M. Ahmed, O. Elashkar, W. Kim, D. R. Kim (2022) Autophagy-mediated degradation of NOTCH1 intracellular domain controls the epithelial to mesenchymal transition and cancer metastasis. Cell Biosci 12:17.
[70] N. Kaludercic, M. C. Maiuri, S. Kaushik, Á. Fernández, J. de Bruijn, F. Castoldi, Y. Chen, J. Ito, R. Mukai, T. Murakawa, J. Nah, F. Pietrocola, T. Saito, S. Sebti, M. Semenzato, L. Tsansizi, S. Sciarretta, J. Madrigal-Matute (2020) Comprehensive autophagy evaluation in cardiac disease models. Cardiovasc Res 116:483-504.
[71] M. S. Willis, C. Patterson (2013) Proteotoxicity and cardiac dysfunction--Alzheimer's disease of the heart? N Engl J Med 368:455-464.
[72] S. Ikeda, D. Zablocki, J. Sadoshima (2022) The role of autophagy in death of cardiomyocytes. J Mol Cell Cardiol 165:1-8.
[73] S. G. Mathiassen, D. De Zio, F. Cecconi (2017) Autophagy and the Cell Cycle: A Complex Landscape. Front Oncol 7:51.
[74] M. Bonora, C. Giorgi, P. Pinton (2022) Molecular mechanisms and consequences of mitochondrial permeability transition. Nat Rev Mol Cell Biol 23:266-285.
[75] D. Denton, T. Xu, S. Kumar (2015) Autophagy as a pro-death pathway. Immunol Cell Biol 93:35-42.
[76] T. P. Neufeld (2012) Autophagy and cell growth--the yin and yang of nutrient responses. J Cell Sci 125:2359-2368.
[77] K. Urbanek, M. C. Cabral-da-Silva, N. Ide-Iwata, S. Maestroni, F. Delucchi, H. Zheng, J. Ferreira-Martins, B. Ogórek, D. D'Amario, M. Bauer, G. Zerbini, M. Rota, T. Hosoda, R. Liao, P. Anversa, J. Kajstura, A. Leri (2010) Inhibition of notch1-dependent cardiomyogenesis leads to a dilated myopathy in the neonatal heart. Circ Res 107:429-441.

[78] V. M. Campa, R. Gutiérrez-Lanza, F. Cerignoli, R. Díaz-Trelles, B. Nelson, T. Tsuji, M. Barcova, W. Jiang, M. Mercola (2008) Notch activates cell cycle reentry and progression in quiescent cardiomyocytes. J Cell Biol 183:129-141.
[79] C. Bongiovanni, F. Sacchi, S. Da Pra, E. Pantano, C. Miano, M. B. Morelli, G. D'Uva (2021) Reawakening the Intrinsic Cardiac Regenerative Potential: Molecular Strategies to Boost Dedifferentiation and Proliferation of Endogenous Cardiomyocytes. Front Cardiovasc Med 8:750604.
[80] N. Pianca, F. Sacchi, K. B. Umansky, *e. al.*, (2022), *Nat Cardiovasc Res*, pp 617–633.
[81] M. S. Ahmed, N. U. N. Nguyen, Y. Nakada, C.-C. Hsu, A. Farag, N. T. Lam, P. Wang, S. Thet, I. Menendez-Montes, W. M. Elhelaly, X. Lou, I. Secco, M. Tomczyk, L. Zentilin, J. Pei, M. Cui, M. Dos Santos, X. Liu, Y. Liu, ..., H. A. Sadek (2024) Identification of FDA-approved drugs that induce heart regeneration in mammals.
[82] R. A. Kore, S. V. Jenkins, A. Jamshidi-Parsian, A. J. Tackett, R. J. Griffin, S. Ayyadevara, J. L. Mehta (2023) Proteomic analysis of transcription factors involved in the alteration of ischemic mouse heart as modulated by MSC exosomes. Biochem Biophys Rep 34:101463.
[83] A. Croquelois, A. A. Domenighetti, M. Nemir, M. Lepore, N. Rosenblatt-Velin, F. Radtke, T. Pedrazzini (2008) Control of the adaptive response of the heart to stress via the Notch1 receptor pathway. J Exp Med 205:3173-3185.
[84] E. Øie, W. J. Sandberg, M. S. Ahmed, A. Yndestad, O. D. Lærum, H. Attramadal, P. Aukrust, H. G. Eiken (2010) Activation of Notch signaling in cardiomyocytes during post-infarction remodeling. Scand Cardiovasc J 44:359-366.
[85] L. Zhao, R. Ben-Yair, C. E. Burns, C. G. Burns (2019) Endocardial Notch Signaling Promotes Cardiomyocyte Proliferation in the Regenerating Zebrafish Heart through Wnt Pathway Antagonism. Cell Rep 26:546-554.e545.

Table 1. Genes upregulated in adult male ErbB2^{tg} mice left ventricles.

FDR	Fold Change	Symbol	Definition
0	1.52	Anxa4	annexin A4 (Anxa4)
0.0007	1.83	App	amyloid beta (A4) precursor protein (App)
0.0177	1.33	Arrb1	arrestin, beta 1 (Arrb1), transcript variant b
0.0929	1.33	Ccnc	cyclin C (Ccnc)
0.1022	1.13	Cdkn1b	cyclin-dependent kinase inhibitor 1B (Cdkn1b)
0.0003	1.24	Egfl7	EGF-like domain 7 (Egfl7), transcript variant c
0.0172	1.48	Epn2	epsin 2 (Epn2)
0.0396	1.48	Epn2	epsin 2 (Epn2)
0.0176	1.45	Epn2	epsin 2 (Epn2)
0.0709	1.33	Fbxw7	F-box and WD-40 domain protein 7, archipelago homolog (Drosophila) (Fbxw7)
0.0006	1.04	Fgf10	fibroblast growth factor 10 (Fgf10)
0.1046	1.7	Hes1	hairy and enhancer of split 1 (Drosophila) (Hes1)
0.0679	1.13	Hey2	hairy/enhancer-of-split related with YRPW motif 2 (Hey2)
0.1787	1.1	Hey2	hairy/enhancer-of-split related with YRPW motif 2 (Hey2)
0.0474	1.46	Heyl	hairy/enhancer-of-split related with YRPW motif-like (Heyl)
0.2332	1.13	Hp	haptoglobin (Hp)
0.1342	1.08	Ift172	intraflagellar transport 172 homolog (Chlamydomonas) (Ift172)
0.0041	1.38	Ift88	intraflagellar transport 88 homolog (Chlamydomonas) (Ift88)
0	1.36	Jag1	jagged 1 (Jag1)
0.1232	1.08	Jag2	jagged 2 (Jag2)
0	1.29	Kctd10	potassium channel tetramerisation domain containing 10 (Kctd10)
0	2.81	Mmp14	matrix metallopeptidase 14 (membrane-inserted) (Mmp14)
0.0236	1.42	Notch4	Notch gene homolog 4 (Drosophila) (Notch4)
0	1.35	Notch4	Notch gene homolog 4 (Drosophila) (Notch4)
0.2203	1.28	Pofut1	protein O-fucosyltransferase 1 (Pofut1), transcript variant 2
0.0421	1.27	Pofut1	protein O-fucosyltransferase 1 (Pofut1), transcript variant 2
0.0209	1.4	Psen1	presenilin 1
0.201	1.33	Reck	reversion-inducing-cysteine-rich protein with kazal motifs (Reck)
0.0264	1	Rfng	RFNG O-fucosylpeptide 3-beta-N-acetylglucosaminyltransferase (Rfng)
0.0003	1.39	Sel1l	sel-1 suppressor of lin-12-like (C. elegans) (Sel1l), transcript variant 1
0.1763	1.14	Six1	sine oculis-related homeobox 1 homolog (Drosophila) (Six1)
0.002	1.5	Slc35c1	solute carrier family 35, member C1 (Slc35c1), transcript variant 2
0	1.53	Sox9	SRY-box containing gene 9 (Sox9)
0.1371	1.31	Stat3	signal transducer and activator of transcription 3 (Stat3), transcript variant 1
0.0001	2.07	Tgfb2	transforming growth factor, beta 2 (Tgfb2)
0.0188	1.33	Tgfbr2	transforming growth factor, beta receptor II (Tgfbr2), transcript variant 1
0	2.55	Tmem100	transmembrane protein 100 (Tmem100)
0.0433	1.48	Traf7	Tnf receptor-associated factor 7 (Traf7)
0.0055	1.15	Zfp423	zinc finger protein 423 (Zfp423)

Table 1. List of genes upregulated in the left ventricles of ErbB2^{tg} mice compared to wild-type littermates (FDR < 0.25).

Table 2. Genes downregulated in adult male mice ErbB2^{tg} left ventricles.

FDR	Fold change	Symbol	Definition
0.0059	-1.22	Adam17	a disintegrin and metallopeptidase domain 17 (Adam17)
0.2056	-1.23	Akt1s1	AKT1 substrate 1 (proline-rich) (Akt1s1)
0.0589	-1.02	Aph1b	anterior pharynx defective 1b homolog (C. elegans) (Aph1b)
0.2421	-1.44	Chac1	ChaC, cation transport regulator-like 1 (E. coli) (Chac1)
0.002	-1.58	Epn1	epsin 1 (Epn1)
0	-1.06	Fgf10	fibroblast growth factor 10 (Fgf10)
0.032	-1.4	Gata2	GATA binding protein 2 (Gata2)
0.0572	-1.23	Itgb1bp1	integrin beta 1 binding protein 1 (Itgb1bp1)
0	-1.25	Kcna5	potassium voltage-gated channel, shaker-related subfamily, member 5 (Kcna5)
0.0253	-1.18	Nfkbia	nuclear factor of kappa light polypeptide gene enhancer in B-cells inhibitor, alpha (Nfkbia)
0.0187	-1.66	Notch3	Notch gene homolog 3 (Drosophila) (Notch3)
0	-2.13	Pgam2	phosphoglycerate mutase 2 (Pgam2)
0.0254	-1.53	Ptp4a3	protein tyrosine phosphatase 4a3 (Ptp4a3)
0	-1.61	Rcan2	regulator of calcineurin 2 (Rcan2), transcript variant 1
0.0002	-1.07	Slc35c2	solute carrier family 35, member C2 (Slc35c2)
0.003	-1.39	Spen	SPEN homolog, transcriptional regulator (Drosophila) (Spen)
0.0185	-1.28	Synj2bp	synaptojanin 2 binding protein (Synj2bp)
0.0021	-1.32	Synj2bp	synaptojanin 2 binding protein (Synj2bp)
0.0023	-1.48	Timp4	tissue inhibitor of metalloproteinase 4 (Timp4)

Table 2. List of genes downregulated in the left ventricles of ErbB2^{tg} mice compared to wild-type littermates (FDR < 0.25).

Figures

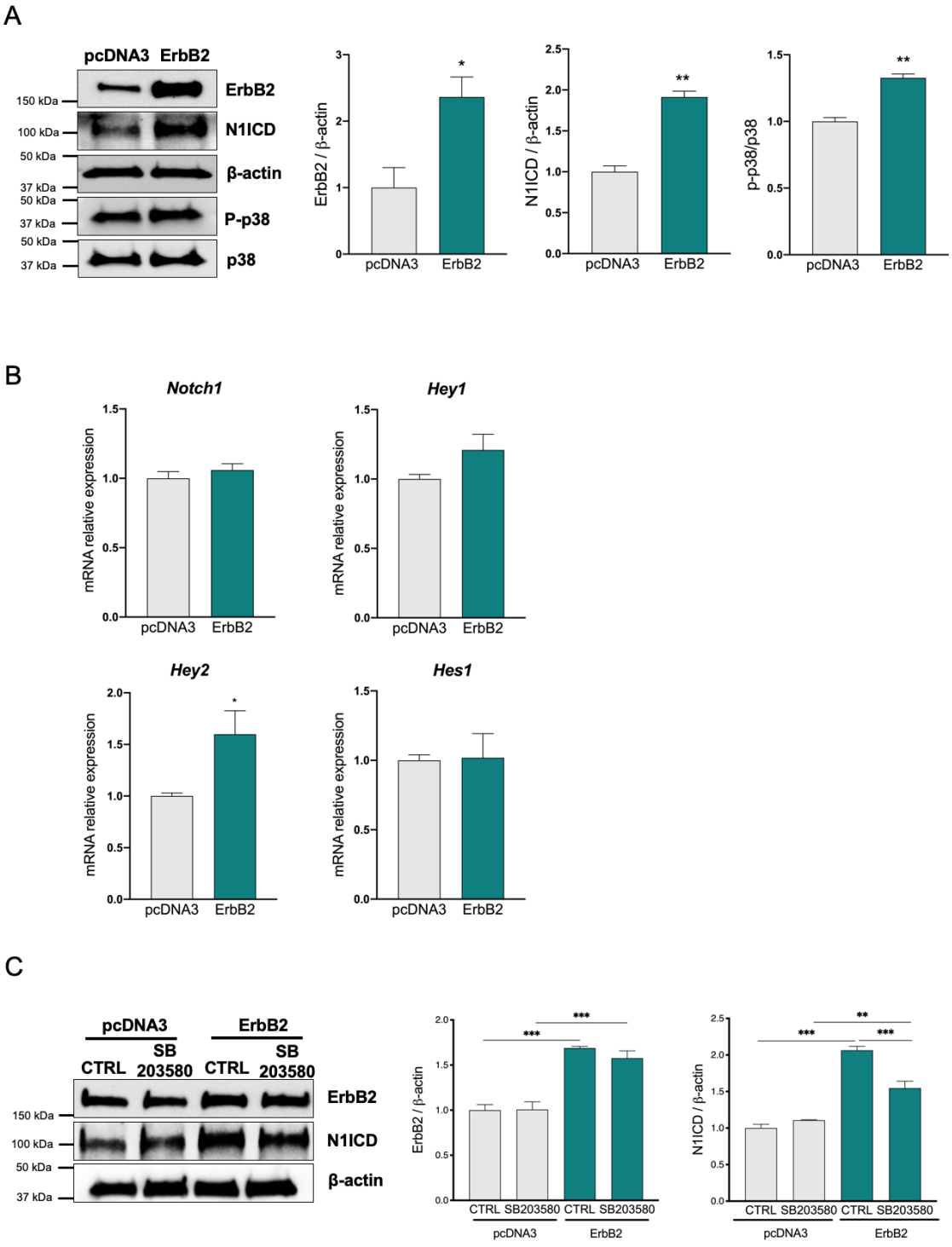

Figure 1. ErbB2 activates Notch1 through a p38-dependent mechanism. H9c2 cells were transfected with a plasmid containing the sequence for ErbB2 or with empty vector as control (pcDNA3) and the following analyses were performed: A) (left) Western blotting analysis of the levels of ErbB2, Notch1 intracellular domain (N1ICD), p-p38 and p38 proteins. β-actin was used as loading control; (right) Densitometric analysis of Western blots showing protein levels after the treatments normalized to untreated control levels, after signal comparison to β-actin. Results are expressed as mean ± SEM of three independent experiments *p < 0.05; ** p < 0.01. B) qRT-PCR analyses were performed to detect *Notch1*, *Hey1*, *Hey2* and *Hes1* mRNA levels in H9c2 cells overexpressing ErbB2. Relative

changes in mRNA expression levels were calculated according to the $2^{-\Delta\Delta Ct}$ method using *Rpl13A* as reference gene. Results are expressed as mean ± SEM of three independent experiments. *p < 0.05. C) (left) Western blotting analysis of the levels of ErbB2 and N1ICD in H9c2 cells transfected with ErbB2 in the presence or absence of a p38 MAPK inhibitor, SB203580 10 μM, for 24h. β-actin was used as loading control; (right) Densitometric analysis of Western blots showing protein levels after the treatments normalized to untreated control levels, after signal comparison to β-actin. Results are expressed as mean ± SEM of three independent experiments. ** p < 0.01; *** p < 0.001.

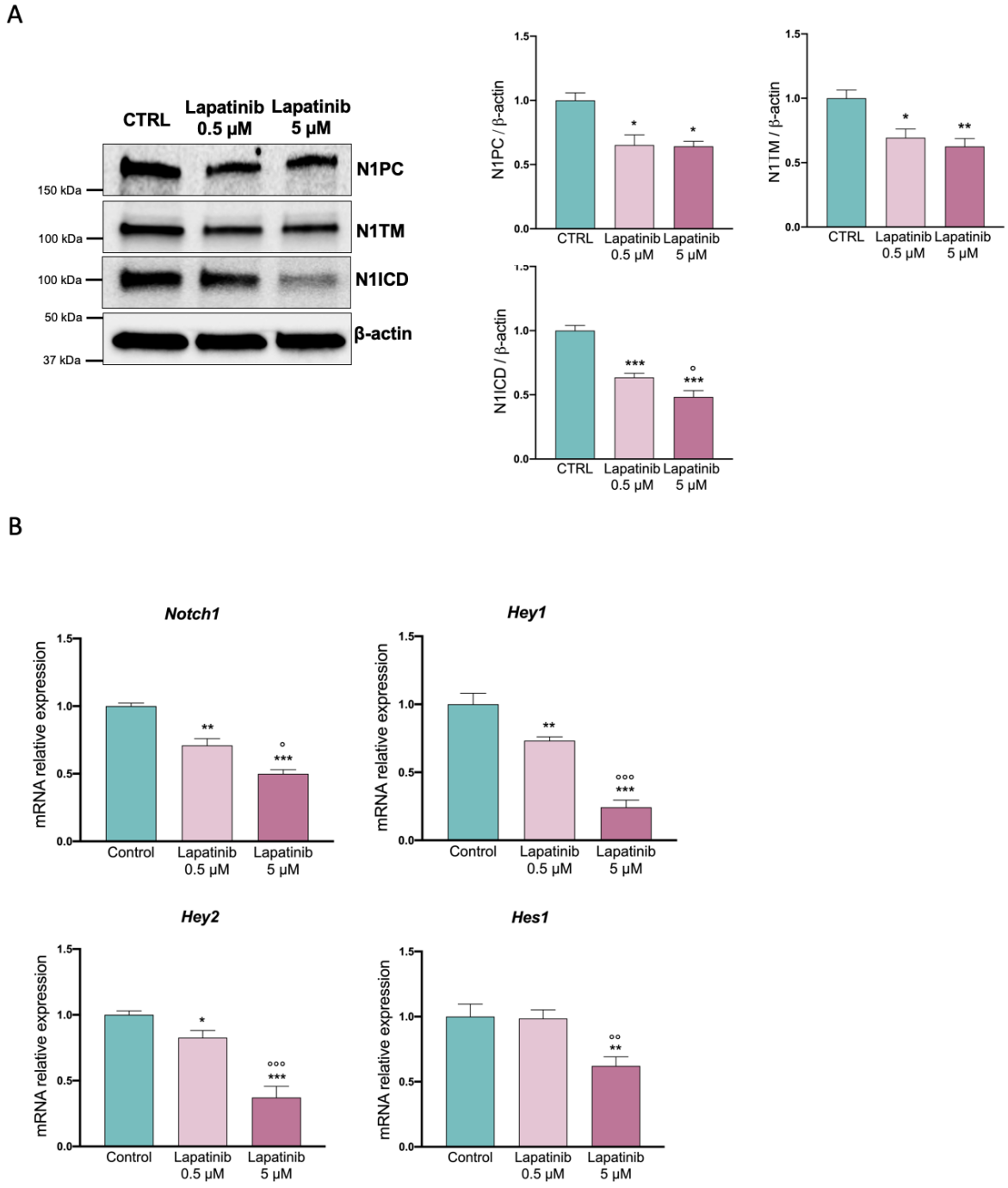

Figure 2. Treatment with lapatinib inhibits Notch1 activation. H9c2 cells were treated with DMSO (CTRL) or lapatinib 0.5 and 5 μM for 24h and the following analyses were performed: A) (left) Western blot analysis of the protein levels of precursor (N1PC), transmembrane (N1TM) and

active form of Notch1 (N1ICD). β-actin was used as loading control; (right) Densitometric analysis of Western blots showing protein levels after the treatment with lapatinib normalized to untreated control levels, after signal comparison to β-actin. Results are expressed as mean ± SEM of three independent experiments. *$p < 0.05$; **$p < 0.01$, ***$p < 0.001$ (pairwise comparison between CTRL and treatments); °$p < 0.05$ (pairwise comparison between lapatinib 0.5 µM and 5 µM). B) qRT-PCR analyses to determine *Notch1*, *Hey1*, *Hey2* and *Hes1* mRNA levels. Relative changes in mRNA expression levels were calculated according to the $2^{-\Delta\Delta Ct}$ method using *Rpl13A* as reference gene. Results are expressed as mean ± SEM of three independent experiments. *$p < 0.05$; **$p < 0.01$; ***$p < 0.001$ (pairwise comparison between CTRL and treatments); °$p < 0.05$; °°$p < 0.01$; °°°$p < 0.001$ (pairwise comparison between lapatinib 0.5 µM and 5 µM).

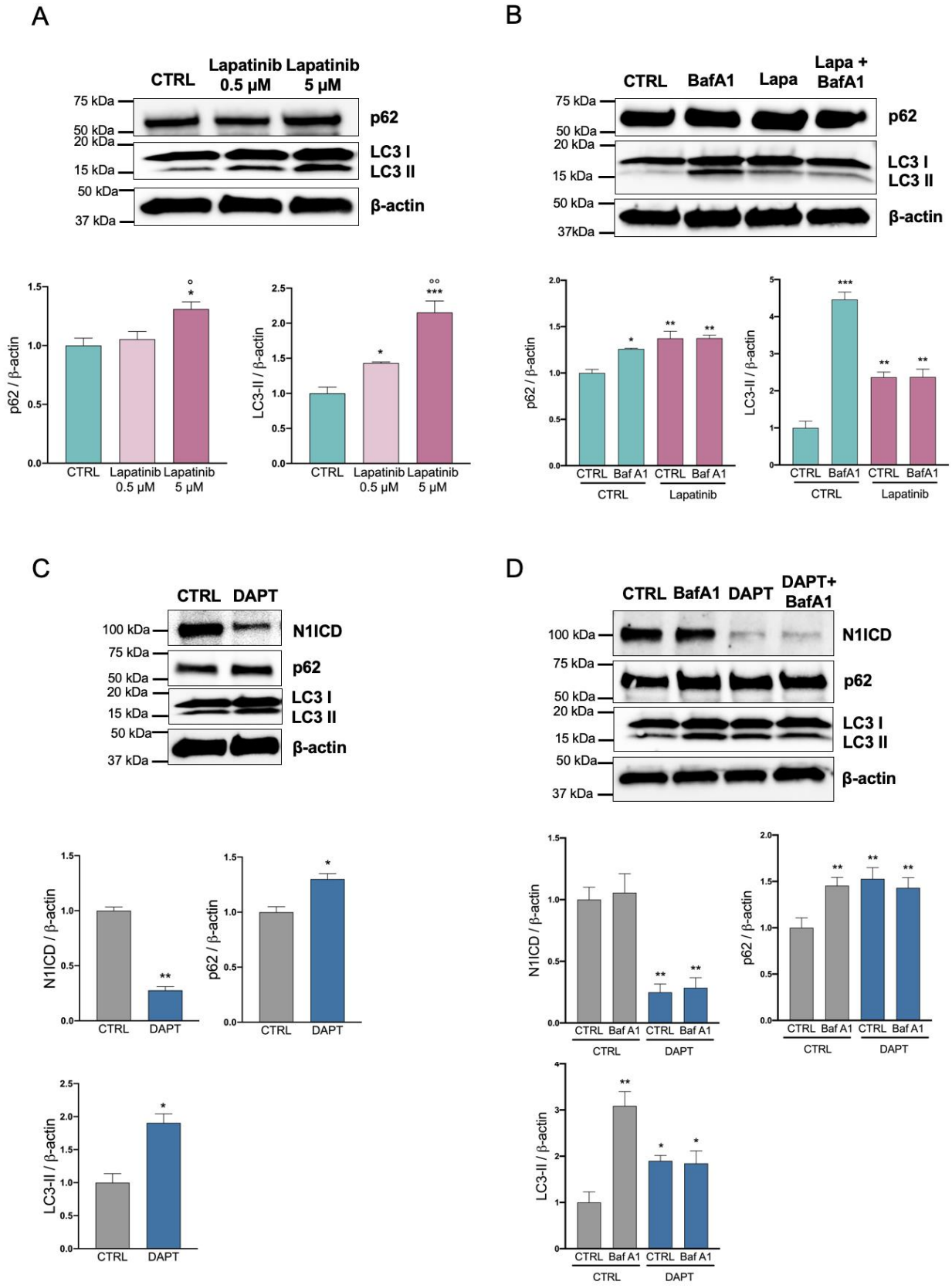

Figure 3. Treatment with lapatinib or with DAPT blocks autophagic flux. A) H9c2 cells were treated with DMSO (CTRL) or lapatinib (Lapa) 0.5 and 5 µM for 24h and were performed Western blot analysis of the protein levels of LC3-I/II and p62. β-actin was used as loading control. Densitometric analysis of Western blots showing protein levels after the treatment with lapatinib

normalized to untreated control levels, after signal comparison to β-actin. Results are expressed as mean ± SEM of three independent experiments. *p < 0.05; ***p < 0.001(pairwise comparison between CTRL and treatments); °p < 0.05; °°p < 0.01 (pairwise comparison between lapatinib 0.5 µM and 5 µM). B) H9c2 cells were treated with lapatinib 5 µM for 24h in the presence or absence of bafilomycin A1 (BafA1) 100 nM during the last 4h of the treatment and, then, Western blot analysis was performed to determine LC3-I/II and p62 protein levels. β-actin was used as loading control. Densitometric analysis of Western blots showing protein levels after the treatments normalized to untreated control levels, after signal comparison to β-actin. Results are expressed as mean ± SEM of three independent experiments. *p < 0.05; **p < 0.01; ***p < 0.001. C) H9c2 cells were treated with DAPT 5 µM for 24h and Western blot analysis was performed to determine N1ICD (active Notch1), p62, and LC3-I/II protein levels. β-actin was used as loading control. Densitometric analysis of Western blots showing protein levels after the treatment with DAPT normalized to untreated control levels, after signal comparison to β-actin. Results are expressed as mean ± SEM of three independent experiments. *p < 0.05; **p < 0.01. D) H9c2 were treated with DAPT 5 µM for 24h in the presence or absence of bafilomycin A1 (BafA1) 100nM during the last 4h of the treatment and Western blot analysis was performed to determine N1ICD, LC3I/II, and p62 protein levels. β-actin was used as loading control. Densitometric analysis of Western blots showing protein levels after the treatments normalized to untreated control levels, after signal comparison to β-actin. Results are expressed as mean ± SEM of three independent experiments. *p < 0.05; **p < 0.01.

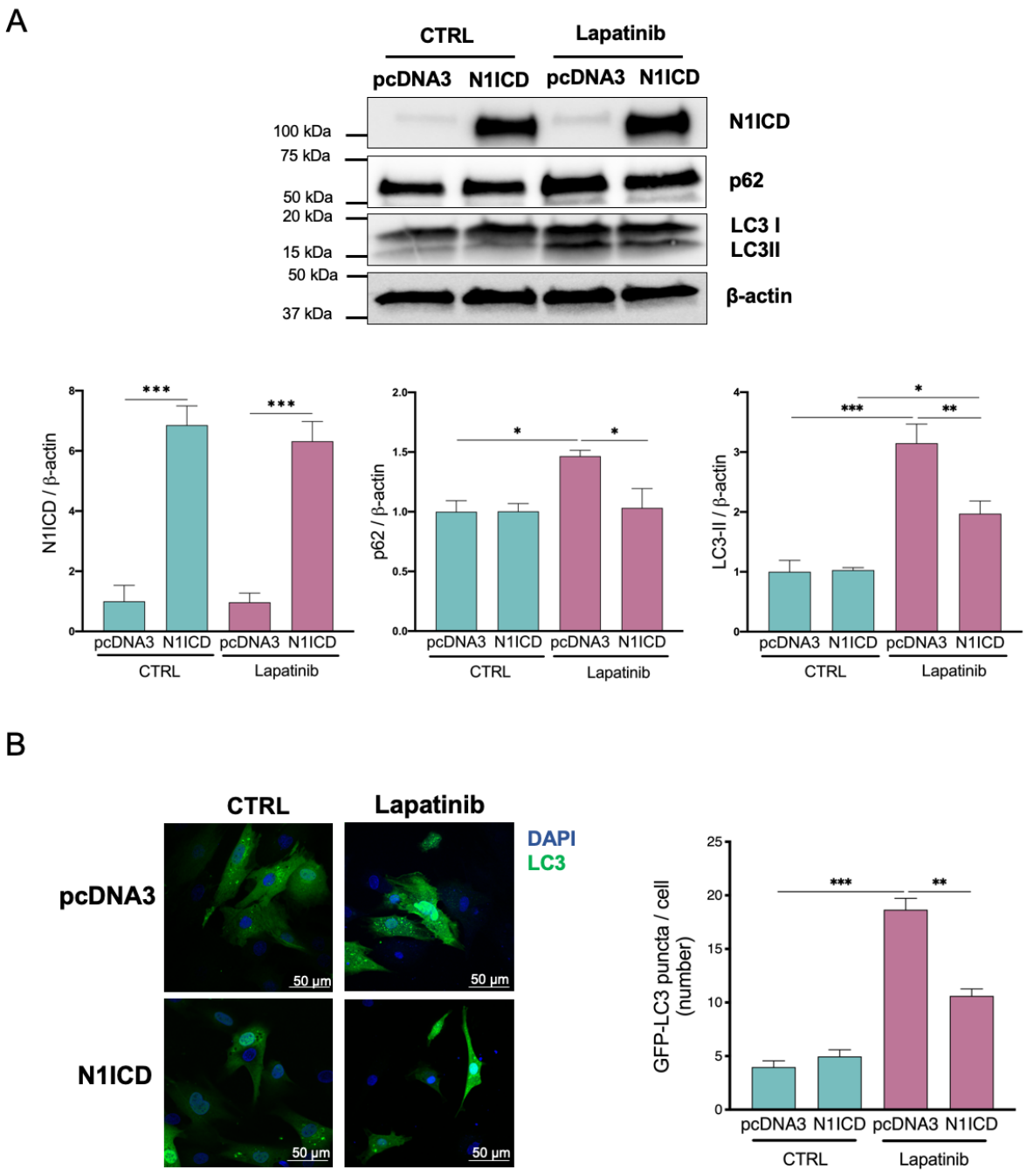

Figure 4. Overexpression of Notch1 rescues autophagic flux impaired by lapatinib treatment. H9c2 cells were transfected with a plasmid encoding the active form of Notch1 (N1ICD) or with empty vector as control (pcDNA3) in the presence or absence of lapatinib 5 μM for 24h and the following analyses were performed: (Top) Western blot analysis of the levels of Notch1 intracellular domain (N1ICD), p62 and LC3-I/II. β-actin was used as loading control. (Bottom) Densitometric analysis of Western blots showing protein levels after the treatments normalized to untreated control levels, after signal comparison to β-actin. Results are expressed as mean ± SEM of three independent experiments. * $p < 0.05$; ** $p < 0.01$; *** $p < 0.001$. B) Detection of autophagy activity through GFP-LC3 puncta (60X magnification). The graph shows the mean number of GFP-LC3 dots per cell counted in 3 visual fields of three independent experiments. Results are expressed as mean ± SEM. ** $p < 0.01$; *** $p < 0.001$.

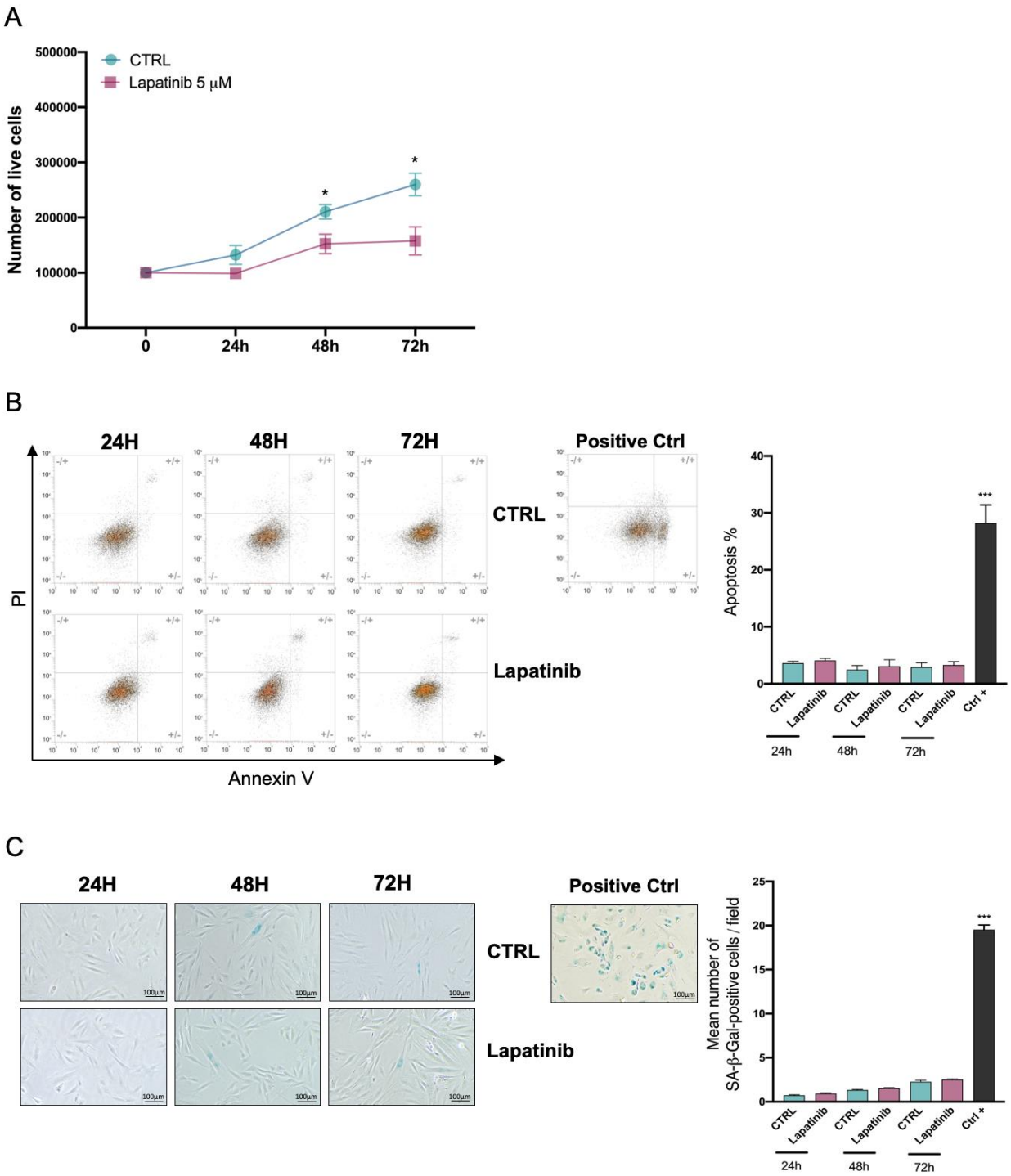

Figure 5. Treatment with lapatinib reduces cell proliferation but does not induce apoptosis or senescence in H9c2 cells. A) H9c2 cells were plated in 6-wells plates and treated with DMSO (CTRL) or lapatinib 5 μM for 24h, 48h and 72h and cell were counted. Results are expressed as a mean ± SEM of three independent experiments. *$p < 0.05$. B) H9c2 cells were treated with DMSO (CTRL) and lapatinib 5 μM for 24h, 48h and 72h and then stained with Annexin V and PI for flow cytometric analysis of apoptosis. (Left) Representative flow cytometry plots are shown for each treatment (+/+ Annexin V-positive PI-positive; +/- Annexin V-positive PI-negative; -/+ Annexin V-negative PI-positive; -/- Annexin V-negative PI-negative). As a technical positive control, H9c2 cells were treated as reported in the Methods section. (Right) Graph shows percentage of apoptotic cells (ratio of Annexin V-positive cells/total cells). Data are expressed as mean ± SEM of three independent

879 experiments. *** $p < 0.001$ (different from any condition). C) H9c2 cells were treated with DMSO
880 (CTRL) and lapatinib 5 μM for 24h, 48h and 72h and then stained with senescence associated β-
881 galactosidase (SA-β-gal) for senescence analysis. (Left) Representative images of SA-β-gal staining
882 and (right) quantification of the blue-stained cells. As a technical positive control, HUVECs were
883 treated as reported in the Methods section. Results are expressed as the mean of SA-β-gal-positive
884 cells counted in 5 visual fields of three independent experiments. *** $p < 0.001$ (different from any
885 condition).
886

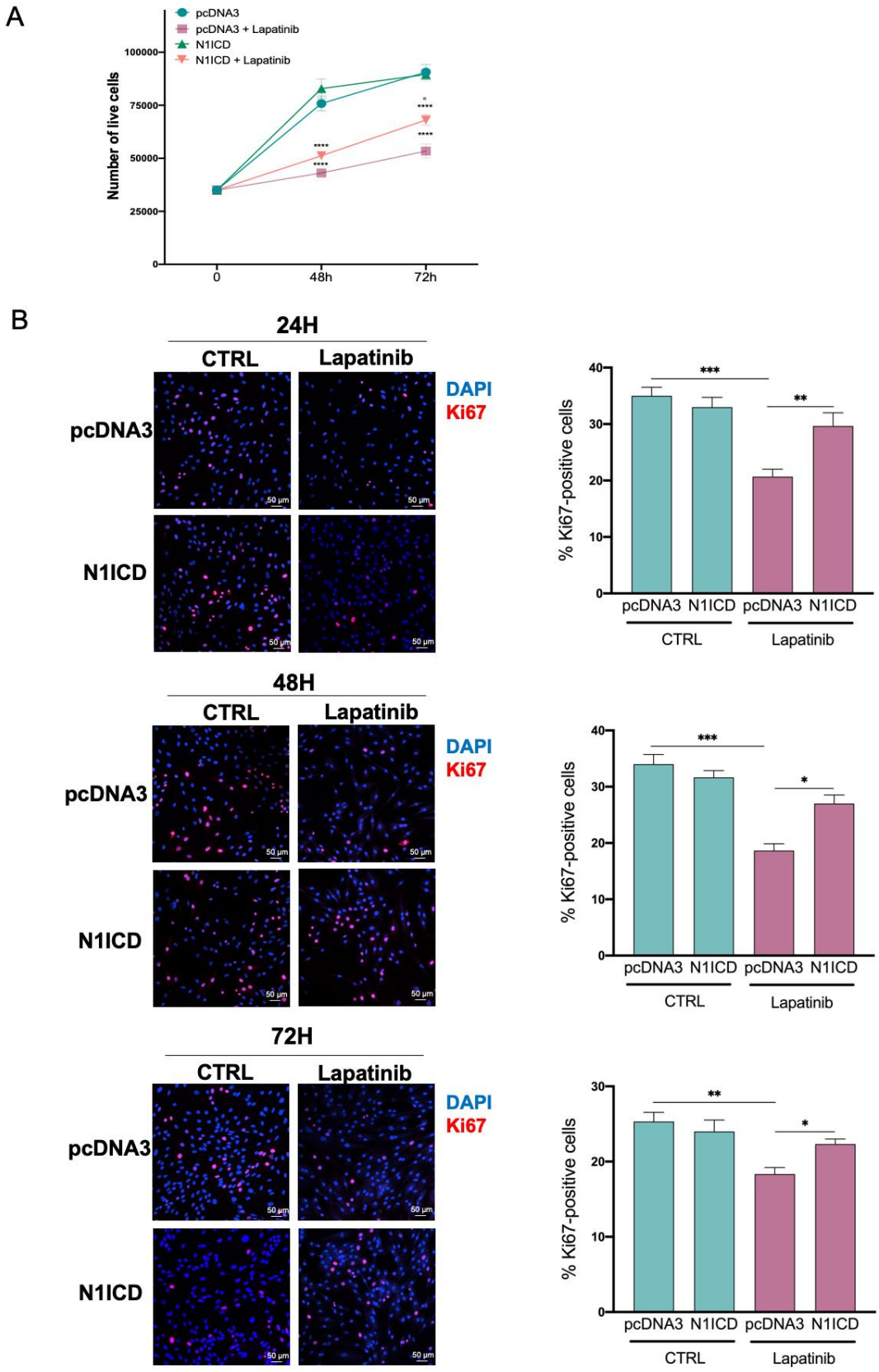

887

888 **Figure 6. Overexpression of Notch1 counteracts the lapatinib-mediated reduction of cell**
889 **proliferation and cell cycle progression.** A) H9c2 were plated in 12-wells plates, transfected with
890 the plasmid containing the sequence for the active form of Notch1, or pcDNA3 (empty vector), then
891 treated with lapatinib 5 µM for 48h and 72h., and cells were counted. Results are expressed as mean
892 ± SEM of three independent experiments. **** $p < 0.0001$; °$p < 0.05$ (pairwise comparison between

plus and minus N1ICD). B) Immunofluorescence staining of Ki67 (red) in H9c2 transfected with active Notch1 (N1ICD) or the empty vector (pcDNA3) in presence or absence of lapatinib 5 μM for 24, 48 and 72h. DAPI (blue) highlights cell nuclei. Graphs show the percentage of Ki67-positive cells counted in 5 visual fields of three independent experiments. Results are expressed as mean ± SEM. * $p < 0.05$; ** $p < 0.01$; *** $p < 0.001$.

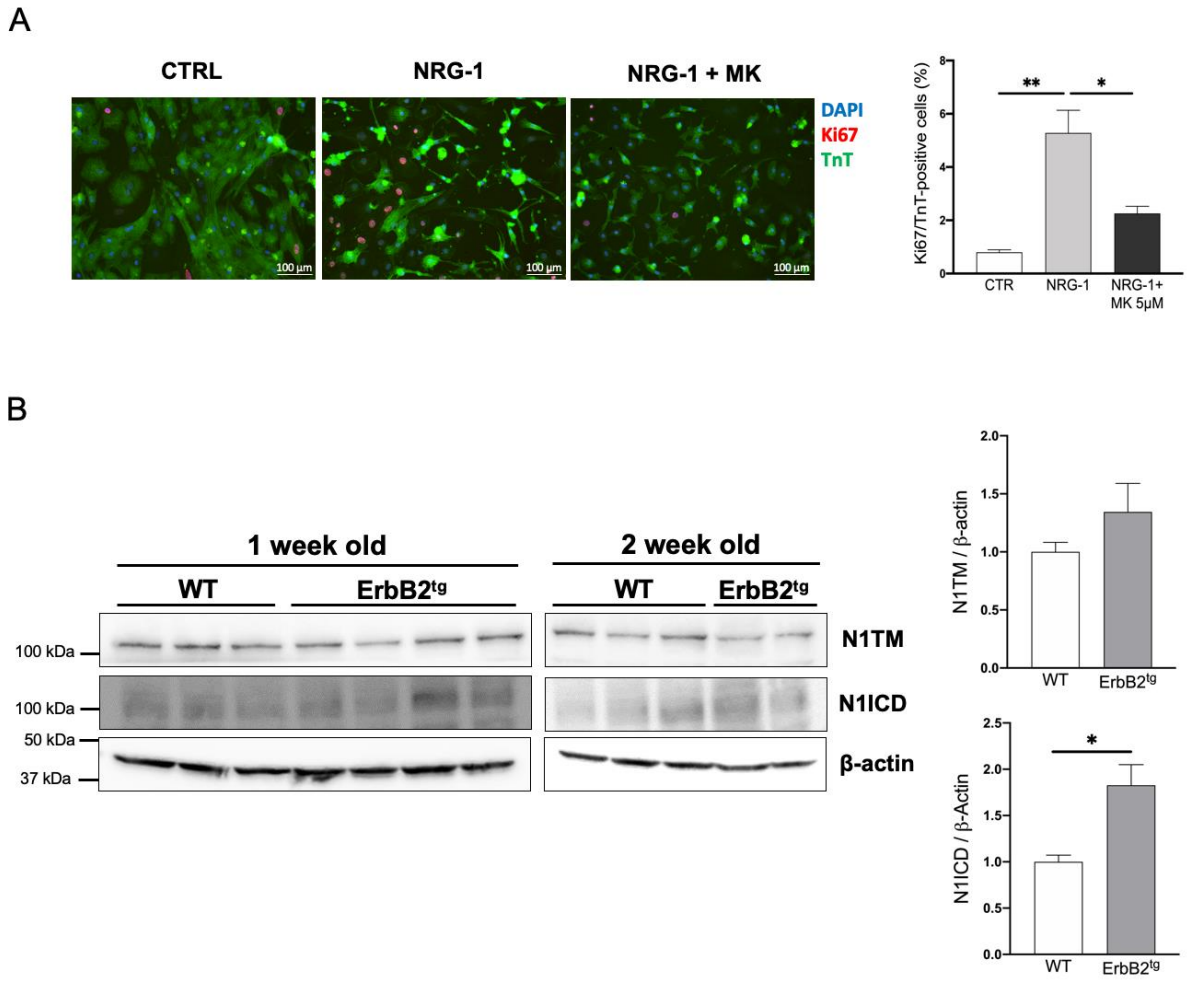

Figure 7. ErbB2 controls Notch1 activation in primary mouse cardiomyocytes and *in vivo*. A) Mouse neonatal cardiomyocytes were treated for 72h with 100 nM neuregulin-1 (NRG-1), in the presence or absence of a Notch inhibitor (5 μM MK0752) and proliferation was assessed by co-staining for Ki67 and cardiac troponin T (TnT). (Left) Representative images (20x magnification) of immunofluorescence staining against Ki67 (red) and cardiac troponin T (green). Nuclei were counterstained with DAPI (blue). (Right) Ki67/TnT double positive cells were counted, and percentage of Ki67/TnT-positive cells was calculated and plotted as mean ± SEM from three independent experiments, *$p < 0.05$; **$p < 0.01$. Tukey's post-hoc test. B) (Left) Hearts of 1 and 2 week of age Her-2/neuT transgenic mice (Tg) overexpressing ErbB2 specifically in cardiomyocytes were lysed and pooled Western blot analysis of the levels of Notch1 transmembrane (N1TM) and cleaved Notch1 (N1ICD) was performed. β-actin antibody was used to ensure equal loading. (Right) Densitometric analysis of Western blots showing protein levels after the treatments normalized to untreated control levels, after signal comparison to β-actin. Results are expressed as mean ± SEM. *$p < 0.05$.

Acknowledgements

The research work presented in this article was supported by Fondo per l'Incentivazione alla Ricerca Dipartimentale (Departmental Research Incentive Fund) FIRD 2022 to PR. The three-year PhD doctorate for PS is co-sponsored by Fondazione Anna Maria Sechi per il Cuore (FASC). PA was supported by the International Society for Heart Research – European Section (ISHR-ES/Servier 2015 Research Fellowship). EL was supported by Italian Society of Cardiology SIC-Merck, Sharp & Dome fellowship. GM is supported by the Italian Ministry of Health grants GR-2018-12367114 and GR-2019-12369862.

Conflict of interest

The authors have no conflicting interests to disclose in relation to this work.

Data availability statement

The data supporting the findings of this study are available from the corresponding author upon reasonable request.

Author contributions

FF, PA, and PR conceived and designed the study. FF, FVDS, PA and PR wrote the manuscript. FF, FVDS, EL, GA, PSS, EB, AA, PS, AWOT, AS, KG and GP performed experiments and analyzed data. FF, FVDS, EL, PSS, KG, GM, SP, PP, RF, ET, PA, and PR contributed to data interpretation and revised the manuscript. All authors read and approved the final manuscript.